ACOUSTICAL INVESTIGATION OF ULTRASOUND CONTRAST AGENTS: THEORY AND EXPERIMENTS

by

Pankaj Jain

A thesis submitted to the Faculty of the University of Delaware in partial fulfillment of the requirements for the degree of Master of Science in Mechanical Engineering

Summer 2006

ACOUSTICAL INVESTIGATION OF ULTRASOUND CONTRAST AGENTS: THEORY AND EXPERIMENTS

by

Pankaj Jain

Approved: _____
Kausik Sarkar, Ph.D.
Assistant Professor in charge of thesis on behalf of the Advisory Committee

Approved: _____
Thomas S. Buchanan, Ph.D.
Chair of the Department of Mechanical Engineering

Approved: _____
Eric W. Kaler, Ph.D.
Dean of the College of Engineering

Approved: _____
Daniel Rich, Ph.D.
Provost, University of Delaware

ACKNOWLEDGMENTS

I would like to thank the members of my thesis committee, my advisor, Dr. Kausik Sarkar, Dr. Ajay Prasad, Dr. Liyun Wang. I would like to thank my parents and my family back in India who always encouraged me for higher studies. I would like to thank my lab mates who have helped me in various stages of my research. I would also like to thank Dr. Dhiman Chatterjee for his help and also for being a part of this research project. I would like to thank my room mates and my friends in Delaware for their support.

I would like to dedicate this thesis to my family in India.

TABLE OF CONTENTS

LIST OF TABLES

LIST OF FIGURES

NOMENCLATURE

A	Air
c	Speed of sound in liquid [m/s]
C	Gas concentration [mol/m^3]
C_g	Gas concentration inside the bubble [mol/m^3]
C_∞	Concentration of the dissolved gas in the liquid very far away from the bubble [moles/m^3]
C_w	Gas concentration at the inner wall of the membrane [mol/m^3]
d	Distance between the transducers [m]
E^s	Dilatational elasticity [N/m]
f	Driving frequency [Hz]
f	Saturation constant
F	Octa- FluoroPropane gas
H_D	Henry's constant
I_{inc}	Intensity of the acoustic field
k	Polytropic constant
k_g	Coefficient of diffusivity of the gas through the liquid [m^2/s]
k_m	Diffusivity of the gas through the membrane [m^2/s]
κ^s	Interfacial dilatational viscosity [msP]
l	Thickness of the membrane [m]
L_g	Ostwald coefficient for the gas

m	Decay constant [min^{-1}]
M	Mass [kg]
p	Pressure [N/m^2]
P_A	Excitation pressure amplitude [MPa]
p_∞	Liquid pressure far away [N/m^2]
P_0	Liquid hydrostatic pressure [N/m^2]
$p_{r=R}$	Pressure in the liquid immediately outside the bubble [N/m^2]
P_s	Scattered pressure [N/m^2]
r	Radial distance [m]
R	Instantaneous bubble radius [m]
$\dot{R}$	Bubble wall velocity [m/s]
R_E	Unstrained radius [m]
R_G	Universal gas constant [J/mol.K]
R_0	Initial bubble radius [m]
t	Time [s]
v_r	Radial component of velocity [m/s]
V_{ref}	Reference signal [volts]
V_{sig}	Signal in the presence of contrast agent [volts]
W_{scat}	Scattered power
X_F	Mole fraction of the osmotic agent
ρ	Liquid density [kg/m^3]
μ	Liquid viscosity [$N\text{-}s/m^2$]
γ	Surface tension [N/m]

γ_0	Reference surface tension at zero area change [N/m]
$\sigma_e^{(l)}$	Extinction cross-section [m^2]
ω	Circular frequency [Hz]
ω_0	Resonance frequency [Hz]
$\alpha(\omega)$	Attenuation in [dB/m]
δ	Damping

ABSTRACT

Ultrasound contrast agents are micron size bubbles used for medical purposes such as diagnostic ultrasound imaging and targeted drug delivery. These bubbles are encapsulated with a shell and have a sparingly soluble gas inside to prevent them from premature dissolution. When these bubbles are excited by the ultrasound they scatter and absorb energy from the sound field, thus leading to the attenuation of the ultrasound signal. In this thesis, we have developed a viscous and a viscoelastic model for the shell. Attenuation measured *in vitro* is compared with model predictions to obtain the characteristic model parameters (surface tension, shell elasticity, dilatational viscosity) for commercially available contrast agents. The viscous model predicts unusually high values of surface tension which motivated the viscoelastic model. We have also used both models to predict the scattered response of microbubbles.

Experimentally measured attenuation is also used to study the growth and destruction of contrast microbubble Definity® (Bristol Meyers Squibb, N. Billerica, MA). Critical pressure amplitudes of ultrasound excitation leading to destruction of contrast microbubbles have been identified for different Pulse Repetition Frequencies (PRFs).

We have developed a model for the growth and dissolution of encapsulated microbubbles taking into account the hindered permeability and elasticity of the encapsulation. We investigated the effects of parameters such as mole fraction of the osmotic agent (inside gas), surface tension, shell permeability, and air saturation level in bulk.

Chapter 1

INTRODUCTION

Ultrasound imaging is the safest and the least expensive modality of medical imaging. The quality of an ultrasound image depends on the difference in reflection of ultrasound from different tissues. A significant improvement of ultrasound blood flow images is obtained by the use of ultrasound contrast agents. Figure 1.1 shows the improvement in the image due to the presence of contrast agents. These agents are micron-size gas bubbles that can navigate through the smallest capillaries (~ 6μm diameter) without obstruction. However, free bubbles of such a small size dissolve quickly due to osmotic diffusion of the gas from inside.

Image without contrast agent

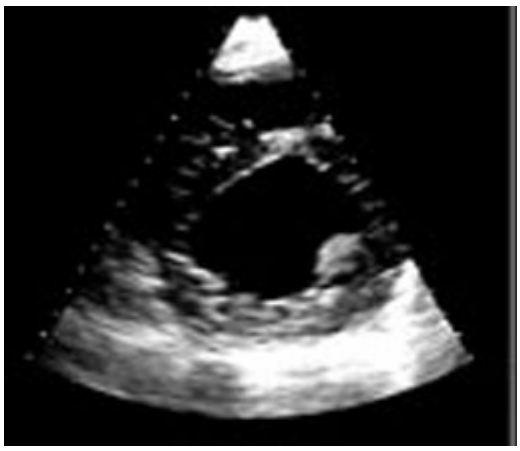

Image with contrast agent

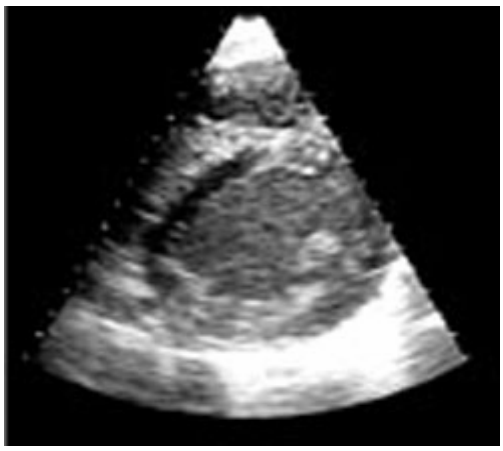

Figure 1.1 Image of a dog's left ventricle without and with contrast agent

Contrast microbubbles are encapsulated by a few-nanometer-thick layer of lipids, proteins or other surface-active materials that stabilizes them against premature dissolution. They are intravenously injected into a patient's body before imaging. The bubbles in the blood reflect more sound than the surrounding tissue and give a clear image of myocardial perfusion (blood flow in the cardiac arteries) during contrast echocardiography (Goldberg et al., 2001; Frinking et al., 2000) .

A number of models for contrast agents have been developed by modifying the free bubble dynamics equation (e.g., Leighton, 1994, p.303) for the presence of encapsulation. de Jong and co-workers (de Jong et al., 1992; de Jong and Hoff, 1993; Frinking and de Jong, 1998) initiated systematic contrast agent modeling with one of the first clinically approved agents, Albunex. They assumed the encapsulating shell to be made of a viscoelastic solid, and used lumped parameters in the free bubble equation to model its effects. Church (1995) provided a detailed theoretical model of contrast agents by treating the encapsulating shell as a nanometer thick layer of an incompressible rubbery medium with shear elasticity and viscosity. He demonstrated the significance of the shell parameters by varying them over a wide range. Introducing slight compressibility and viscoelasticity of the surrounding liquid in the same model, Khismatullin and Nadim (2002) performed a theoretical analysis to conclude that these effects are less important than that of the encapsulation. Morgan et al. (2000) used a modified Herring equation with a similar model for the encapsulation to compare with optical observations obtained by a high-speed digital camera.

In this thesis, we have developed a viscous and a viscoelastic model for the encapsulation. Corresponding Rayleigh-Plesset equations for the bubble dynamics are

obtained, and the characteristics model parameters experimentally determined. The model predictions are compared with experiments.

1.1 Suitability of broadband attenuation for determination of model parameters for the contrast agent

Scattering and absorption of sound energy by contrast agents lead to the attenuation of the ultrasound signal. The performance of contrast agents *in vivo* depends on their interaction with the incident acoustic pressure. The encapsulation plays a significant role in this interaction. The stabilizing encapsulation is modeled as a layer (infinitesimal thickness) or an interface with material properties such as interfacial viscosity, elasticity and surface tension. The single bubble model is fitted to the measured attenuation data along with a population size distribution to estimate these material properties (de Jong and Hoff, 1993; Hoff et al, 2000; Chatterjee and Sarkar, 2003; Sarkar et al., 2005).

Recently, Chen et al. (2002) have studied the effects of the excitation amplitude on attenuation through contrast agents Optison® (GE Health Care, Princeton, NJ) and Definity. They found that the broadband attenuation curves depend on the center frequency of the excitation pulse. They concluded that "results showed great inconsistency when the center frequency of the incident broadband pulse was changed, indicating that broadband techniques may not be suitable for contrast-agent attenuation measurements". They attributed the behavior to the nonlinear response of the bubbles to a broadband signal.

In this thesis, we carefully investigate the issue of dependence of attenuation on the center frequency of excitation, the excitation amplitude and the

concentration of microbubbles. Typically, attenuation versus frequency relations are based on a linear propagation theory (Chatterjee et al., 2005) and do not depend on excitation amplitude. We discuss our experimental results in view of the linear theory of attenuation, and determine the limit on pressure amplitudes above which the linearity breaks down, and thereby establish the range where traditional attenuation-frequency curves can be meaningfully used for acoustic characterization.

1.2 Destruction of ultrasound contrast agents

Strong ultrasound pulses of large amplitude and higher power can destroy these microbubbles by rupturing the encapsulation. Microbubble destruction is useful in real time blood flow velocity measurement (Sonne et al., 2003; Porter et al., 2001), stimulating arteriogenesis (Song et al., 2002) or targeted drug delivery (Shohet et al., 2000; Price et al., 1998; Porter et al., 1996). In each application after microbubbles are intravenously injected, they are destroyed in a specific tissue region by an ultrasound pulse. The blood velocity can be estimated from the time it takes for bubbles to reappear in the region after they are ultrasonically destroyed. Destruction of microbubbles stimulates growth of new blood vessels in the region (arteriogenesis). The bubbles can be functionalized so that it preferentially attaches to a target tissue, e.g. tumors, and then burst to destroy the tumor. They can also be coated with drugs and genes that can be released to the tumor upon destruction, without serious side effects. Shohet et al. (2000) were able to deliver adenoviral trangene to a rat myocardium through ultrasound mediated microbubble destruction.

Destruction of a particular contrast agent depends on numerous factors such as exciting pulse, liquid temperature, hydrostatic pressure or amount of dissolved

gas in the blood. Destruction is studied by several researchers (Porter et al., 1995; Walker et al., 1997; Klibanov et al., 1998; Dayton et al., 1999; Shi et al., 2000; Moran et al., 2000; Sboros et al., 2001; Chomas et al., 2000; Chomas et al., 2001; Klibanov et al., 2002; Chen at al., 2003). Two distinct mechanisms have been suggested for bubble destruction—slow gas diffusion and fast fragmentation. While varying the excitation, it was found that there is a threshold on the strength of the excitation that is needed for destruction. The threshold excitation was found to be different for different contrast agents due to the difference in strength of the encapsulation as well as solubility of the gas content in the surrounding liquid.

Klibanov et al. (2002) studied destruction of Albunex® and Optison® microbubbles and found that Albunex is more prone to loss of echogenicity than Optison. They concluded that the gas inside plays a more important role than the shell as Optison has sparingly soluble perfluoropropane gas whereas Albunex is air-filled. Moran et al. (2000) and Sonne et al. (2003) however observed that Optison destruction rate is much faster than Definity® though they have similar high-molecular weight gas core. They ascribed this difference to the difference in shell composition—Definity® with a lipid layer showed more resistance as compared to albumin-coated Optison. Shi et al. (2000) observed that acoustic pressures causing microbubble destruction for one agent are usually not necessarily the same for another agent.

In this thesis we use time dependent ultrasound attenuation measurements to study the growth and destruction of contrast microbubble Definity® at varying pressure amplitudes for various PRF's (Pulse Repetition Frequency). We determine the

threshold pressure for the bubble break up. Slow gas diffusion and faster fragmentation of the bubbles have been identified to cause different characteristics in attenuation.

1.3 Growth and dissolution of contrast microbubbles

When a microbubble is excited with low intensity ultrasound the shell of the bubble forms defects (Dayton et al., 1999). Typically the diffusivity of gas inside the bubble is lower than that of the air. This causes sudden ingress of air from the outside into the bubble at the initial stages of diffusion, causing the bubble to grow. Bubble growth and dissolution have been studied by many researchers theoretically and experimentally. Dissolution of an air bubble has been studied by Epstein and Plesset (1950). Kabalnov et al. (1998) and Chen et al. (2002) studied the dissolution by modifying the Epstein-Plesset equation by having two different gases inside the free bubble. Kabalnov et al. (1998) studied the effects of varying surface tension and initial mole fraction of the inside gas. Shi et al. (2000) and Chatterjee et al. (2005) experimentally studied bubble growth by acoustic means. Borden et al. (2002) investigated the effects of encapsulation by putting an ad hoc resistance in their dissolution model.

Here we develop a model for diffusion of gas from a contrast microbubble with two gases—air and octa-fluoropropane (OFP). Specifically we provide a rational model for the effects of encapsulation—hindered permeability and elasticity. We study bubble growth and dissolution using this model by varying parameters such as mole fraction of OFP, surface tension, shell permeability, shell elasticity and air saturation level in the bulk (water).

1.4 Layout of the thesis

In chapter 2, we discuss the structure of ultrasound contrast agents, their persistence, and the physics of Contrast Echocardiography (CE). We describe the viscous and the viscoelastic models of encapsulation used to represent the acoustic response of contrast microbubbles. The theory of attenuation and scattering from them is also delineated. We develop a model of gas diffusion from contrast microbubbles to describe growth and dissolution. Chapter 3 describes various experimental setups used to measure attenuation and scattering. It also explains the methodology used to determine the model parameters for a contrast agent. Chapter 4 presents the results from experimental measurement and numerical simulation. The suitability of the attenuation measurement to characterize contrast microbubbles is discussed. The characteristic parameters for Definity microbubbles are obtained analyzing the attenuation data. We discuss the ultrasound induced destruction of Definity. The model predictions for growth and dissolution of microbubbles are presented. Finally, Chapter 5 summarizes the thesis and points towards future research.

Chapter 2

THEORETICAL BACKGROUND

This chapter describes the theoretical background for the dynamics of contrast microbubbles. It also includes the theoretical information about the attenuation and scattering of ultrasound by these contrast microbubbles.

2.1 Ultrasound Contrast Agents

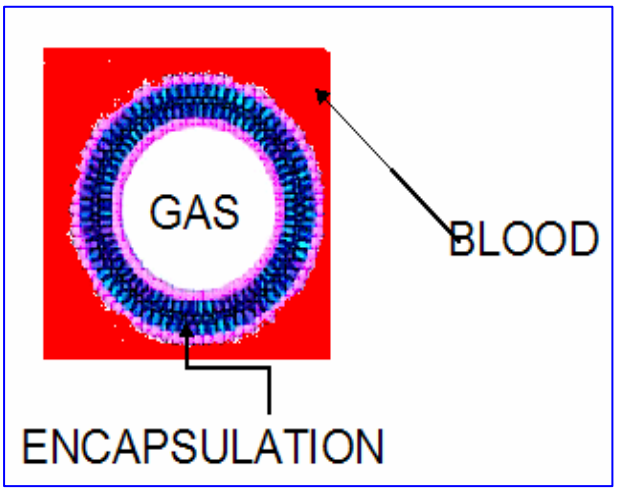

Figure 2.1 Schematic of ultrasound contrast agent

Contrast microbubbles are micron size gas bubbles encapsulated by a shell (Figure 2.1). The shell prevents bubbles from premature dissolution. Less soluble gas is chosen to prevent diffusion of the gas. Some of the commercially available contrast agents are shown in Table 2.1.

Table 2.1: Commercially available contrast agents and their features

Contrast Agent	Gas	Nature of encapsulation	Size (μm)
Optison	Octafluoropropane	Albumin	2-4.5
Sonazoid	Perfluorocarbon	Surfactant	3
Definity	Octafluoropropane	Phospholipid	1.1-3.3

2.2 Contrast echocardiography (CE) physics

The mechanism of CE is based on the physical principles of rarefaction and compression created by an US wave insonicating the bubble (Figure 2.2). Rarefaction occurs with reduction in pressure of the gas when struck by the negative portion of the acoustic wave, and compression refers to the rise in pressure of a medium struck by the positive portion of the acoustic cycle (Figure 2.2). Compression and rarefaction lead to volume pulsations of microbubbles and it is this change that results in the CE signal. Excitation of these microbubbles is mentioned in terms of Mechanical Index (MI), which is defined as peak rarefactional pressure in MPa (i.e., peak negative pressure) divided by the square root of the US frequency MHz. The range of MI for clinical purposes is between .05-1.9. For low MI (0.1), the microbubbles undergo linear oscillations. When MI is increased (0.2 to 0.7), nonlinear oscillations occur. Destruction of microbubbles occurs to some degree at all mechanical indices; it is extensive at MI of 0.8 to 1.9.

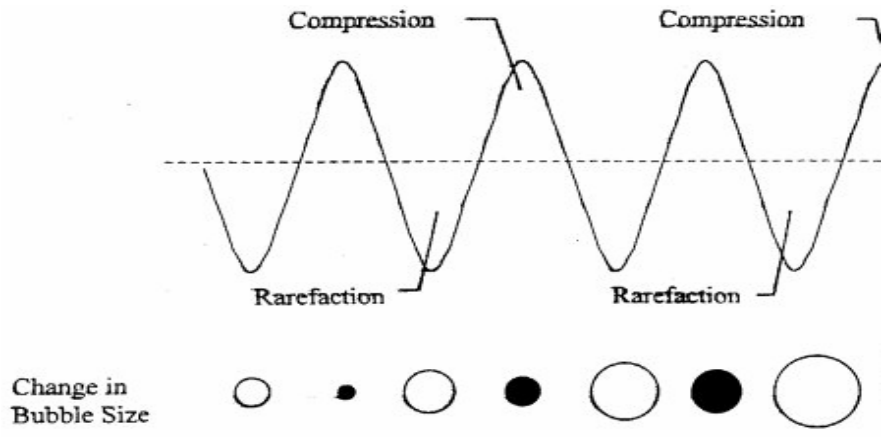

Figure 2.2 Cycles of compression and rarefaction when the bubble is excited

2.3 Size distribution of Definity® microbubbles

The size distribution of microbubbles in a Definity sample was measured using a Coulter Counter (Model Z-2, Beckman Coulter Instruments, Florida) in our lab. The measurement was performed immediately after the sample was prepared and also after 5 hours. In the intervening period the sample was left undisturbed.

Figure 2.3 shows that there is no significant change in the mean size of the bubble (1.99 μm and 1.87 μm respectively) though there is a reduction in the total number of bubbles from 3.12×10^9/ml to 1.62×10^9/ml. For comparison, we also measured the size distribution optically with an Olympus BH-2 microscope in conjunction with a Canon MVC-300 digital camera. Photos were taken in light transmission mode (Figure 2.4).

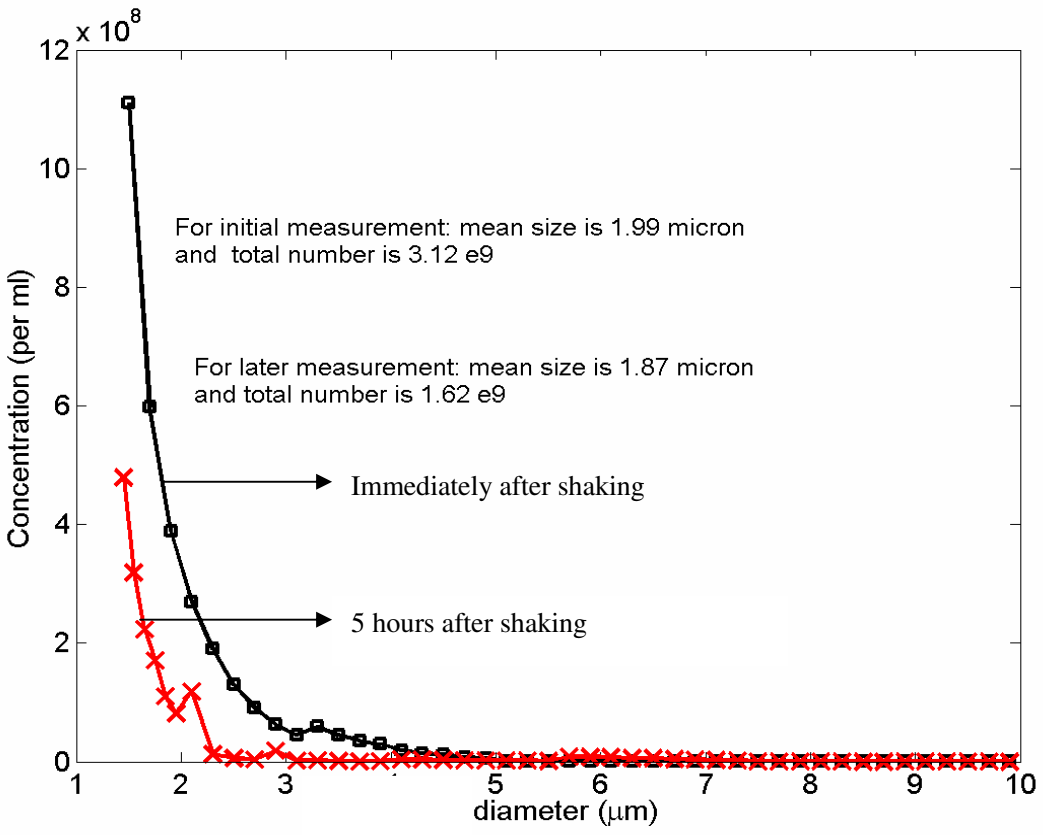

Figure 2.3 Bubble size distribution at 2 times, immediately after shaking and after 5 hours (Chatterjee et al., 2005)

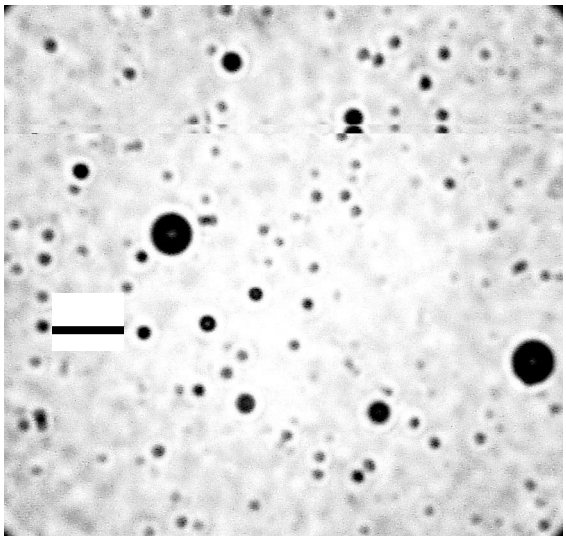

Figure 2.4 Optical image of Definity under microscope, the bar indicates 10 micron.

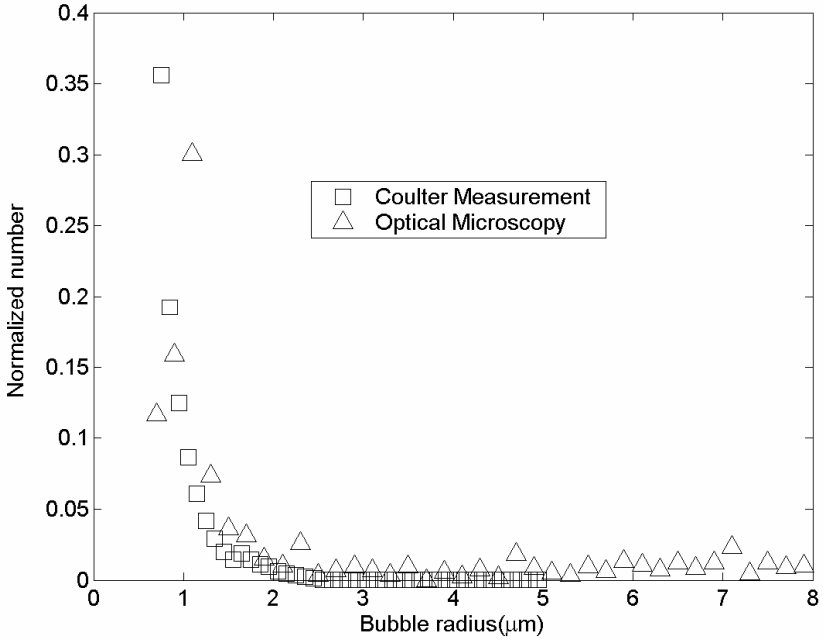

Figure 2.5 Comparison of size distribution measurement using Coulter counter and optical microscope.

Figure 2.5 shows that the size distributions measured optically and by the Coulter counter compare well with each other providing credence to the reliability of the measuring procedure.

2.4 Bubble as a spring mass damper system

Bubbles can be treated as a spring mass damper system, and can be compared to a bob of certain mass attached to a spring. The spring, which provides the restoring force, models the gas within the bubble. All the viscous terms act as dampers, such as the viscosity of the surrounding liquid, the shell viscosity, etc. Care must be taken with this analogy, however when considering the inertia, because in case of the bob the body is more dense than the surrounding medium (air), whilst in the case of the bubble the body is less dense than its surrounding medium. In the spring–bob system, inertial and momentum effects are dominated by the mass of the bob, the inertial effects associated with the motion of the surrounding fluid (air) being negligible. In contrast, with the bubble, it is the inertia associated with the motion of the surrounding fluid which dominates the inertia, the mass of the gas within the bubble being negligible. So we apply the mass and momentum conservation equations for the surrounding liquid (see, Leighton, 1994).

2.5 Governing mass and momentum equations and bubble dynamics:

2.5.1 Viscous Newtonian model

We model the interface as a shell of infinitesimal thickness because the shell is only a few molecules thick. Assuming spherical symmetry, the mass and momentum conservation equations in the surrounding liquid, which is assumed to be incompressible, are

$$\frac{1}{r^2}\frac{\partial}{\partial r}(r^2 v_r) = 0 \tag{2.1}$$

$$\rho\left(\frac{\partial v_r}{\partial t} + v_r\frac{\partial v_r}{\partial r}\right) = -\frac{\partial p}{\partial r} + \mu\left[\frac{1}{r^2}\frac{\partial}{\partial r}(r^2\frac{\partial v_r}{\partial r}) - \frac{2v_r}{r^2}\right] \tag{2.2}$$

where v_r is the radial component of velocity, r is the radial distance, ρ the liquid density, p the pressure, and μ the liquid viscosity. From mass conservation Eq. (2.1) and the boundary condition at $r = R$, $v_r = \dot{R}$, the radial velocity in the liquid is readily obtained as

$$v_r = \dot{R}R^2 / r^2 \tag{2.3}$$

$\dot{R}$ is the bubble wall velocity while R is the instantaneous bubble radius. Note that the velocity being irrotational, the viscous terms vanish in Eq. (2.2). Using Eq. (2.3), Equation (2.2) can be integrated to give at $r=R$

$$\rho\left(R\ddot{R} + \frac{3}{2}\dot{R}^2\right) = p_{r=R} - p_\infty, \tag{2.4}$$

where $p_{r=R}$ is the pressure in the liquid immediately outside the bubble, and p_∞ is liquid pressure far away:

$$p_\infty = P_0 - P_A \sin\omega t, \tag{2.5}$$

P_0 is the liquid hydrostatic pressure, $\omega=2\pi f$ with f being the driving frequency, and P_A is the acoustic pressure amplitude. The dynamic boundary condition at the bubble interface relates the pressure $p_{r=R}$ to the bubble dynamics. The total stress $\underline{\underline{\sigma}}$ in the liquid outside is given by a Newtonian relation

$$\underline{\underline{\sigma}} = -p\underline{\underline{\delta}} + \underline{\underline{\tau}} \ , \tag{2.6}$$

where p is the pressure, $\underline{\underline{\delta}}$ the identity tensor, and $\underline{\underline{\tau}}$ the viscous part of the stress. Since we assume the flow to be spherically symmetric, we only consider the radial component of the stress

$$\tau_{rr}\big|_{r=R} = 2\mu \frac{\partial v_r}{\partial r}\bigg|_{r=R} = -\frac{4\mu \dot{R}}{R} \ , \tag{2.7}$$

using Eq. (2.3). The pressure inside is related with the total radial stress outside through a jump at the interface:

$$\left(-p + 2\mu \frac{\partial v_r}{\partial r}\right)_{r=R} + P_G \equiv -p_{r=R} - 4\mu \frac{\dot{R}}{R} + P_G = \frac{2\gamma}{R} + \frac{4\kappa^s \dot{R}}{R^2} \ , \tag{2.8}$$

or

$$p_{r=R} = P_G - 4\mu \frac{\dot{R}}{R} - \frac{2\gamma}{R} - \frac{4\kappa^s \dot{R}}{R^2} \tag{2.9}$$

where γ is the surface tension, κ^s is the interfacial dilatational viscosity. The surface shear viscosity does not appear due to the spherical symmetry of the dynamics. The (dilatational) viscous term can be explained by noting that the bubble undergoes area dilation at a rate $A^{-1}dA/dt = 2\dot{R}/R$, ($A = 4\pi R^2$). It results in a uniform tension of magnitude $2\kappa^s \dot{R}/R$ in Eq. (2.8), in addition to the surface tension γ. In an undisturbed

condition (zero motion), using $p_{r=R} = P_0$ from (2.8) we obtain the initial gas pressure inside the bubble:

$$P_{G0} \equiv P_G(t=0) = P_0 + \frac{2\gamma}{R_0}, \tag{2.10}$$

where R_0 is the initial radius. Note that p_{G0} is not in equilibrium with the outside pressure P_0. The gas pressure inside the bubble is assumed to vary with bubble volume polytropically with k as the polytropic exponent :

$$P_G R^{3k} = P_{G0} R_0^{\ 3k}. \tag{2.11}$$

R_0 is the initial radius. We have chosen k = 1, corresponding to an isothermal gas behavior inside the bubble; the bubble size is too small for diffusion to be important at the time scale (10^{-6} s) of oscillation. From Eq (2.4) we arrive at the modified Rayleigh-Plesset type model or the viscous newtonian model :

$$\rho(R\ddot{R} + \frac{3}{2}\dot{R}^2) = P_{G0}\left(\frac{R_0}{R}\right)^{3k} - 4\mu\frac{\dot{R}}{R} - \frac{2\gamma}{R} - \frac{4\kappa^s\dot{R}}{R^2} - P_0 + P_A \sin\omega t \tag{2.12}$$

This viscous Newtonian model Eq. (2.12) has surface tension γ and the shell dilatational viscosity κ^s as unknowns which are to be determined through measurement.

2.5.2 Viscoelastic model for the shelled microbubble

With the Newtonian rheology (Eq. (2.12)), the encapsulation is purely viscous and is characterized by γ and κ^s. We will see in chapter 4 that such a model for the encapsulation results in an unusually high value for the surface tension. The value for the surface tension should be less than the value for the clean air water interface due to adsorption of small amount of surface active materials. In an encapsulation the

molecules are however at a high concentration and closely packed, with a strong attractive interaction between them. Due to the attractive interaction, any change in area will lead to an elastic force, a phenomenon commonly known as Gibb's elasticity (see Evans and Skalak, 1980, pp. 80 and 86 and Edwards et al., 1991, pp. 118 and 172). Chatterjee et al. (2005) introduced a viscoelastic model, which takes care of the elastic nature of the shell. In the viscoelastic model we have a dilatational elasticity (E^s) term along with the surface tension term. Edwards et al. (1991, p118) has shown that dilatational surface elasticity or Gibb's elasticity can also be treated as effects arising from surface tension gradients. Accordingly, the dilatational elasticity E^s is introduced as

$$E^s = \left(\frac{\partial \gamma}{\partial \beta}\right)_{\beta=0}, \qquad \gamma = \gamma_0 + E^s \beta, \tag{2.13}$$

where $\beta = \delta A / A = [(R / R_E)^2 - 1]$ is the fractional change in area from *equilibrium* that represents an unstrained equilibrium condition (denoted by unstrained radius R_E). γ_0 is the reference surface tension at zero area change. With the modification to surface tension γ, the dynamic boundary condition (2.9) at $r = R$ becomes

$$p_{r=R} = P_G - 4\mu \frac{\dot{R}}{R} - \frac{4\kappa^s \dot{R}}{R^2} - \frac{2\gamma_0}{R} - \frac{2E^s}{R}\left[\left(\frac{R}{R_E}\right)^2 - 1\right] \tag{2.14}$$

At the initial zero motion state, the inside pressure satisfies

$$P_{G0} = P_0 + \frac{2\gamma_0}{R_0} + \frac{2E^s}{R_0}\left[\left(\frac{R_0}{R_E}\right)^2 - 1\right]. \tag{2.15}$$

In contrast to the Newtonian rheology [see Eq. (2.10)], we assume an *equilibrium of pressure* inside and outside the bubble $P_{G0} = P_0$, that ensures stability of

microbubbles, even if the encapsulation is permeable to the gas. Imposing pressure equilibrium, we obtain the equilibrium radius from Eq. (2.15) to be

$$R_E = R_0\left(1-\frac{\gamma_0}{E^s}\right)^{-\frac{1}{2}}. \tag{2.16}$$

The resulting Rayleigh-Plesset equation in contrast to Eq. (2.12) takes the form:

$$\rho\left(R\ddot{R}+\frac{3}{2}\dot{R}^2\right)=P_{G0}\left(\frac{R_0}{R}\right)^{3k}-4\mu\frac{\dot{R}}{R}-4k^s\frac{\dot{R}}{R^2}-\frac{2\gamma_0}{R}-\frac{2E^S}{R}\left[\left(\frac{R}{R_E}\right)^2-1\right]-P_0+P_A\sin\omega t \tag{2.17}$$

2.6 Attenuation of ultrasound by contrast microbubbles

Attenuation is the amount of energy being absorbed and scattered by the contrast microbubbles when excited by the ultrasound. Attenuation is derived following a linear theory. For small oscillation $R=R_0+X$, one can linearize equation (2.17) or (2.12) in X to obtain a damped simple harmonic oscillator:

$$\ddot{X}+\frac{\dot{X}}{\rho R_0^{\,2}}\left(4\mu+\frac{4\kappa^s}{R_0}\right)+\frac{X}{\rho R_0^{\,2}}\left(3kP_0-\frac{4\gamma_0}{R_0}+\frac{4E^s}{R_0}\right)=\frac{P_A}{\rho R_0}\sin\omega t\,, \tag{2.18}$$

or

$$\ddot{X}+\frac{\dot{X}}{\rho R_0^{\,2}}\left(4\mu+\frac{4\kappa^s}{R_0}\right)+\frac{X}{\rho R_0^{\,2}}\left[3kP_0-\frac{2\gamma}{R_0}(3k-1)\right]=\frac{P_A}{\rho R_0}\sin\omega t\,, \tag{2.19}$$

respectively for viscous and viscoelastic models. The corresponding resonance frequencies are

$$\omega_0^{\,2}=\frac{1}{\rho R_0^{\,2}}\left(3kP_0-\frac{4\gamma_0}{R_0}+\frac{4E^s}{R_0}\right) \text{ and } \omega_0^{\,2}=\frac{1}{\rho R_0^{\,2}}\left[3kP_0+\frac{2\gamma}{R_0}(3k-1)\right]. \tag{2.20}$$

The damping term is the same for both models and has an additional dilatational interfacial term compared to the free bubble case (Hoff et al., 2000; Medwin, 1977):

$$\delta_{total} = \delta_{liquid} + \delta_{interface} + \delta_{radiation}$$

$$\delta_{liquid} = \frac{4\mu}{\rho\omega_0 R_0^{\,2}}, \qquad \delta_{interface} = \frac{4\kappa^s}{\rho\omega_0 R_0^{\,3}}, \qquad \delta_{radiation} = \frac{\omega^2 R_0}{\omega_0 c} \tag{2.21}$$

We have assumed the surrounding liquid to be incompressible, and thereby do not obtain the radiation damping terms in (2.18) or (2.19) . However, including it by the standard prescription (2.21) does not change the parameter values by more than 1%. The extinction cross-section $\sigma_e^{(l)}$ for the linearized dynamics is:

$$\sigma_e^{(l)} = 4\pi R_0^{\,2} \frac{c\delta_{total}}{\omega_0 R_0} \frac{\Omega^2}{\left[(1-\Omega^2)^2 + \Omega^2 \delta_{total}\right]} \tag{2.22}$$

where $\Omega = \omega/\omega_0$ and c is the sound speed in the surrounding liquid (see, e.g., Sarkar and Prosperetti, 1994).

The power absorbed and scattered by microbubbles in the frequency domain leads to attenuation $\alpha(\omega)$ in dB/distance

$$\alpha(\omega) = 10\log_{10} e \int_{a_{\min}}^{a_{\max}} \sigma_e(a;\omega) n(a) da \tag{2.23}$$

where e is the base of natural logarithm, $n(a)da$ is the number of bubbles per unit volume with radius in $(a, a+da)$, and $a_{max(min)}$ is the maximum (minimum) value of the range of bubble radii. For the case of N bubbles per unit volume of a uniform size the integral simplifies to $N\sigma_e$. Notice that $\alpha(\omega)$ is a function of the unknown bubble parameters (γ, κ^s) or $(\gamma_0, E^s, \kappa^s)$. The method to determine these bubble parameters have been discussed in chapter 3 and results presented in chapter 4.

2.7 Scattering of ultrasound by contrast microbubbles

When the acoustic wave is incident on an obstacle, the obstacle reflects the incident wave. This phenomenon is known as scattering. The acoustic pressure P_s scattered by a bubble is nonlinear and is given by (Brennen 1995):

$$P_s(r,t) = \rho \frac{R}{r}(2\dot{R}^2 + R\ddot{R}) \tag{2.24}$$

where ρ is the density of the liquid, r is the radial distance, R is a instantaneous bubble radius. Once the scattered pressure is calculated, we compute the FFT of the scattered pressure and obtain the different harmonics. We can also calculate the scattering cross-section given by:

$$\sigma_s = W_{scat} / I_{inc} \tag{2.25}$$

where W_{scat} is the scattered power, and I_{inc} is the intensity of the acoustic field. These quantities are given by:

$$W_{scat} = 4\pi \left\langle r^2 P_s(t)^2 \right\rangle_T / (\rho c) \tag{2.26}$$

$$I_{inc} = \left\langle P_A(t)^2 \right\rangle_T / (\rho c) \tag{2.27}$$

where c is the liquid sonic velocity and $\langle \ \rangle_T$ is the average of a quantity over a time interval T, $P_A(t)$ is the incident acoustic pressure.

2.8 Growth and dissolution of contrast microbubbles

We model the bubble shell as a semi-permeable membrane, with two gases—air and octafluoropentane (OFP)—inside the bubble. The dissolution time scale and the growth of the bubbles are studied for varying mole fraction of the osmotic agent

(OFP), surface tension, shell permeability, and air saturation level in the bulk. Also, an elastic shell is considered. Here we assume that the process of dissolution is very slow and hence dissolution by steady diffusion is considered. Note that the bubble growth and dissolution can be significantly affected by ultrasound excitation, which is not considered here.

2.8.1 Steady diffusion of gas through the permeable shell of a microbubble

Neglecting the unsteady effects of time scale R^2/k_g, the gas concentration C outside the bubble of radius R satisfies the steady mass diffusion equation, which in a spherically symmetric case is

$$\frac{1}{r^2}\frac{\partial}{\partial r}(r^2\frac{\partial C}{\partial r})=0, \tag{2.28}$$

with the boundary condition $C \to C_\infty$ as $r \to \infty$. C_∞ is the concentration of the dissolved gas in the liquid far from the bubble. The boundary condition at the liquid side of the bubble wall is that the flux in the liquid side is matched by diffusion through the membrane:

$$-k_g \left.\frac{\partial C}{\partial r}\right|_R = h\left[C_w - C(R)\right], \tag{2.29}$$

where C_w is the gas concentration at the inner wall of the membrane in contact with the gas inside and $C(R)$ is the gas concentration at the outer wall of the membrane. The mass flux through the membrane is modeled by a coefficient h which can be estimated as

$$h = \frac{k_m}{l} \ , \tag{2.30}$$

where k_m is the diffusivity of the gas through the membrane and l is the thickness of encapsulation. Such a model is appropriate for a thin membrane as considered here. Solving (2.28) with boundary condition (2.29) we obtain

$$C(r) = \frac{R^2(C_w - C_\infty)}{r\left(\frac{k_g}{h} + R\right)} + C_\infty . \tag{2.31}$$

The bubble contains gas at a concentration C_g. Its growth is determined by the mass flux at the bubble wall

$$\frac{dM}{dt} = \frac{d}{dt}(\frac{4}{3}\pi R^3 C_g) = 4\pi R^2 k_g \left.\frac{\partial C}{\partial r}\right|_R . \tag{2.32}$$

We assume that the membrane is completely hydrated. Therefore, the dissolved gas concentration C_w at the membrane wall in contact with the inside gas is related to the inside gas concentration by the Ostwald coefficient $C_w = L_g C_g$. Note that for an ideal gas, it is also equivalent to the Henry's law, where $C_w = H_D^{-1} p_g$ relates to the gas partial pressure p_g, which in turn is proportional to the concentration C_g by the gas law. Using Eq. (2.31), we obtain for evolution of bubble radius:

$$\frac{d(R^3 C_g)}{dt} = 3R^2 k_g \frac{(C_\infty - L_g C_g)}{\left(\frac{k_g}{h} + R\right)}. \tag{2.33}$$

2.8.2 Multiple gases

Due to the presence of air inside the bubble as well as dissolved in the liquid outside, we have to consider diffusion of two components, air A and the sparingly

soluble gas F, which is called an osmotic agent. We correspondingly get two equations for these two components. We assume $C_F(\infty)=0$, i.e. the gas is only introduced into the liquid through the bubbles. $C_A(\infty)$ is determined by the fact that the liquid is in contact with air at atmospheric pressure p_{atm}, i.e. $C_A(\infty)=fL_A p_{\text{atm}}/R_{\text{G}}T$. R_G is the universal gas constant. The factor f describes whether the liquid is saturated ($f=1$), undersaturated ($f<1$) or oversaturated ($f>1$) with air.

The two equations are then

$$\frac{d(R^3C_F)}{dt}=-3Rk_F\frac{L_FC_F}{\left(\frac{k_F}{h_FR}+1\right)}\ , \tag{2.34}$$

$$\frac{d(R^3C_A)}{dt}=3Rk_AL_A\frac{\left(f\frac{p_{\text{atm}}}{R_GT}-C_A\right)}{\left(\frac{k_A}{h_AR}+1\right)}\ . \tag{2.35}$$

Note that for $h_{A,F}\to\infty$ or more appropriately for the nondimensional number $h_{A,F}R/k_{A,F}\to\infty$, we obtain the same equations as that by Kabalnov et al. (1998) in absence of the membrane. The pressure inside the bubble arising from partial pressures due to the osmotic agent and the air is higher than the atmospheric pressure by the Laplace pressure due to surface tension γ:

$$p_A+p_F=(C_A+C_F)R_GT=p_{\text{atm}}+\frac{2\gamma}{R}\,. \tag{2.36}$$

Following Kabalnov et al. (1998), we non-dimensionalize variables:

$$\hat{\gamma}=\frac{2\gamma}{p_{atm}R_0};\hat{R}=\frac{R}{R_0};\lambda=\frac{k_A}{k_F}$$

$$A = \widehat{R}^3 \frac{C_A R_G T}{P_{atm}}; F = \widehat{R}^3 \frac{C_F R_G T}{P_{atm}}; \tau = \frac{k_F}{R_0^2} t \ ,$$

where R_o is the initial bubble radius $R(t=0)$. Equations (2.34), (2.35) and (2.36) become

$$\frac{dF}{d\tau} = \frac{-3L_F F}{\widehat{R}\left(\frac{k_F}{h_F R_0} + \widehat{R}\right)} \ , \tag{2.37}$$

$$\frac{dA}{d\tau} = \frac{-3\lambda L_A (A - f\widehat{R}^3)}{\widehat{R}\left(\frac{k_A}{h_A R_0} + \widehat{R}\right)} \ , \tag{2.38}$$

$$F + A = \widehat{R}^3 + \widehat{\gamma}\widehat{R}^2 \ . \tag{2.39}$$

With initial conditions

$$\widehat{R}(0) = 1, \qquad A(0) + F(0) = 1 + \widehat{\gamma}, \qquad \frac{F(0)}{A(0) + F(0)} = X_F. \tag{2.40}$$

X_F is the mole-fraction of the sparingly soluble gas F.

Without solving the equations, one can note several features of the problem. Because the concentration of the osmotic agent is assumed to be zero far away form the bubble, Eq. (2.37) indicates that the osmotic agent steadily diffuses out of the bubble leading to $F \to 0$. In contrast, nonzero air concentration far away allows a steady state for Eq. (2.38) With pressure equilibrium Eq. (2.39) we then obtain

$$A = f\widehat{R}^3 \qquad \text{and} \qquad A = \widehat{R}^3 + \widehat{\gamma}\widehat{R}^2 ,$$

with a solution only for $f \geq 1$:

$$\widehat{R} = \frac{\widehat{\gamma}}{f-1} .$$

Surface tension causes the inside pressure to exceed the outside pressure Eq. (2.39), and drives air and the osmotic agent out of the bubble, except when the liquid is oversaturated. Indeed, the above equation indicates several routes for enhancing the bubble lifetime: (1) by decreasing Ostwald coefficient L_F, i.e. using a less soluble osmotic agent, (2) reducing the surface tension γ, (3) decreasing the shell permeability h_F. All of them have been identified in the literature. However, there is another aspect of the encapsulation, viz., elasticity, which also acts against the surface tension and therefore promotes stability.

2.8.3 Shell elasticity

The above model is appropriate for a free bubble with the interface characterized by a surface tension γ. However, as mentioned before the mirobubbles are stabilized by an encapsulation made of surface active materials such as proteins, lipids or ordinary surfactants. Surface active materials nominally reduce the surface tension of the absorbed interface (and thereby stabilizing the bubble). Furthermore, the encapsulation acts as an elastic layer. There have been various models of the viscoelastic encapsulation. Such elasticity can also be modeled as a Gibb's elasticity term arising from the gradient of surface tension with respect to fractional area change (Edwards et al, p118):

$$E^s = \left(\frac{\partial \gamma}{\partial \beta}\right)_{\beta=0}, \qquad \gamma = \gamma_0 + E^s \beta, \qquad \beta = \delta A / A = [(R / R_E)^2 - 1] \tag{2.41}$$

E^S is the dilatational surface elasticity and R_E the equilibrium radius. The pressure balance Eq. (2.36) then becomes

$$(C_A + C_F)R_G T = P_A + P_F = P_{atm} + \frac{2\gamma_0}{R} + \frac{2E^S}{R}\left[\left(\frac{R}{R_E}\right)^2 - 1\right] \tag{2.42}$$

The elastic term gives rise to a restoring stress away from the equilibrium radius R_E, and is positive or negative depending on whether the bubble radius is more or less than the equilibrium value. This should be contrasted with the surface tension term which is of the same sign for all values of the radius. Initially the bubbles are made in a solution saturated with the insoluble gas (typically perfluorocarbon). Therefore, we can assume that the bubbles are stabilized having an equal pressure inside and outside, leading to

$$\frac{2\gamma_0}{R_0} = -\frac{2E^S}{R_0}\left[\left(\frac{R_0}{R_E}\right)^2 - 1\right] \qquad \text{or} \qquad R_E = R_0\left(1 - \frac{\gamma_0}{E^S}\right)^{-1/2} \tag{2.43}$$

Note that such equilibrium is possible only for the case of $E^s \geq \gamma_0$. Alternatively, especially for smaller elasticity, we assume that the initial area is at its equilibrium value. With this model we arrive at a modified non-dimensional surface tension term and a new non-dimensional elasticity term

$$\hat{\gamma} = \frac{2\gamma_0}{P_{atm}R_o}, \qquad \hat{E} = \frac{2E^S}{P_{atm}R_o}.$$

Equations (2.39) becomes

$$F + A = \hat{R}^3 + \hat{\gamma}\hat{R}^2 + \hat{E}\hat{R}^2\left(\frac{\hat{R}^2}{\hat{R}_E{}^2} - 1\right) \tag{2.44}$$

So, we use equations (2.44), (2.37), (2.38) and the initial conditions in equation (2.40) to study the effects of elasticity on the growth and dissolution of the microbubbles. The results for the inclusion of elasticity have been discussed in chapter 4.

Chapter 3

EXPERIMENTAL SET-UPS AND METHOD

3.1 Set-up for measurement of attenuation of ultrasound

Broadband attenuation measurement has been widely used for characterizing ultrasound contrast agents (UCA). Attenuation theory is a linear theory. Attenuation should not depend upon the excitation pressure amplitude. It has been found that the use of attenuation at higher pressure amplitudes for characterization is not feasible. We investigated to validate the range of pressure amplitudes suitable for the use of attenuation for characterization of the contrast microbubbles. We have also conducted attenuation experiments to study the growth and dissolution or destruction of these microbubbles.

Attenuation experiments have been carried out with two setups. A schematic of the attenuation set-up 1 is shown in Figure 3.1. A pulser-receiver (model 5800, Panametrics, Waltham, MA, USA) was used to excite an unfocused broadband transducer at a PRF of 100 Hz. It transmitted a single-cycle pulse of length 1μ-sec into the bath. Three different broadband transducers were used with center frequencies of 2.25, 3.5 and 5 MHz. The -6dB bandwidth for these transducers are 1.58-2.95 MHz, 2.5-4.99 MHz and 3.13-6.19 MHz respectively.

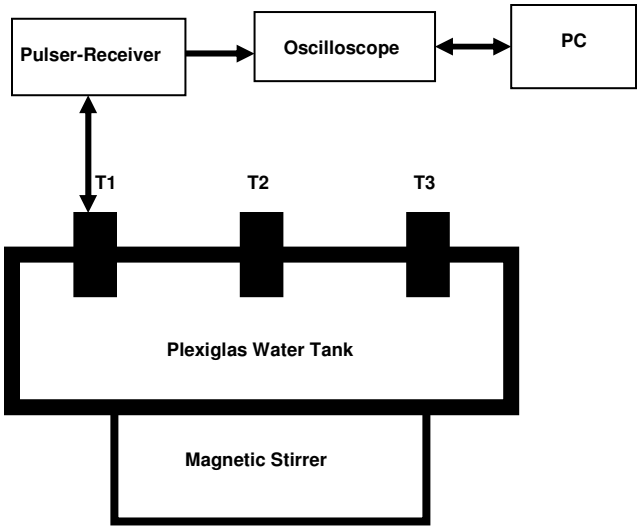

Figure 3.1 Attenuation set-up 1 with three transducers T1, T2, T3.

Ultrasound travels through the tank containing the contrast agent solution and the signal reflected from the back wall is received by the same transducer. The total travel path was 8.2 cm. The received signal was amplified by the pulser-receiver and fed into an oscilloscope (TDS2012, Tektronix, OR, USA) and a computer. Matlab® (Math-work Inc, Natick, MA, USA) was used for postprocessing of the data. A 0.4 mm needle hydrophone (PZT-Z44-0400, Onda Corporation, CA, USA) was used to measure the acoustic pressure. The lowest value of the peak negative excitation amplitude produced by this set-up using the pulser-receiver was 0.67 MPa. To obtain lower excitation amplitudes, we used an in-line tunable dB-attenuator (0-60dB, model 432D, Kay Elemetrics Corporaton, NJ, USA) between the pulse-receiver and the transducer. A part of the data was also obtained using a second set-up, where a function generator (33250A, Agilent, Palo Alto, CA, USA) and a power amplifier (ENI A150,

Rochester, NY, USA), as shown in Figure 3.2, were used to produce one-cycle bursts. In these experiments, we used an unfocused broadband 5 MHz transducer as transmitter, and another unfocused broadband transducer with 3.5 MHz center frequency was used as receiver. Both were mounted on the wall of a bath and were separated by a distance of 10.5 cm.

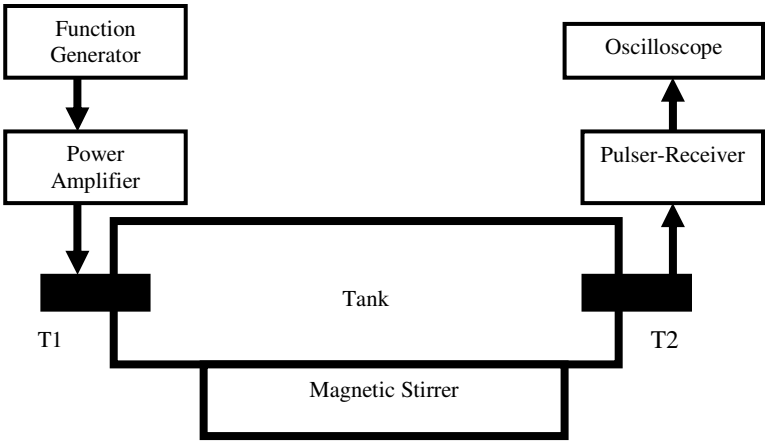

Figure 3.2 Attenuation set-up 2

The second set-up has been used to also study the growth and dissolution of these microbubbles. The two set-ups have been found to produce the same result within the variability accepted between different realizations of the same experiments.

The contrast agent used in these experiments was Definity. Definity microbubbles were prepared by shaking the suspension in a Vial-Mix™ (Bristol-Myers Squibb Medical Imaging, North Billerica, MA, USA) for 45 s according to the manufacturer's recommendations. 2 min after the preparation the bubble suspension was injected into a phosphate buffer solution (Isoton-II, Beckman Coulter, FL, USA).

Excitation was started 1 min after injection. A magnetic stirrer (Fisher Scientific) was used to produce a homogeneous solution containing microbubbles.

In a typical experiment, the received signal was recorded before Definity was introduced into the solution to obtain a reference signal V_{ref}. Then the measurement was repeated after injection of Definity into the solution to find the signal V_{sig} in presence of contrast agent. For each measurement, 64 sequences of signals were averaged in the oscilloscope and then transferred to a PC via an IEEE-488 (GPIB) interface for further analysis. The data transfer was controlled using Labview® (National Instruments, Austin, TX, USA). From the measured data, attenuation is computed:

$$\alpha(\omega) = 10\log_{10}\left(\frac{V_{ref}^{\ 2}(\omega)}{V_{sig}^{\ 2}(\omega)}\right)/d \tag{3.1}$$

where $\alpha(\omega)$ is in dB/cm, d is the distance between the receiver and the transmitter and $V_{ref}(\omega)$ and $V_{sig}(\omega)$ are the received sound in the absence and presence of contrast agents, respectively. With a plane linear wave assumption, different frequency components of a broadband pulse travel independently of each other:

$$P(x,t) = \mathrm{Re}\, P_0 e^{i\omega(t-x/c)} e^{-\frac{\alpha(\omega)}{2}x}, \qquad I(x) = \left|P(x,t)\right|^2 = I_0 e^{-\alpha(\omega)x} \tag{3.2}$$

Re indicates the real part, P_0 and I_0 are the incident pressure amplitude and intensity, and c is the sound speed in the liquid. ω is the circular frequency and $\alpha(\omega)$ is the attenuation per unit distance.

3.2 Set-up for measurement of scattering of ultrasound

We measure scattering of ultrasound by Definity® at different pressure amplitudes, and investigate the fundamental (response at f_0, the same frequency as that of the excitation) and subharmonic (response at $f_0/2$) scattered responses (see chapter 4). Continuous excitation was used for these experiments.

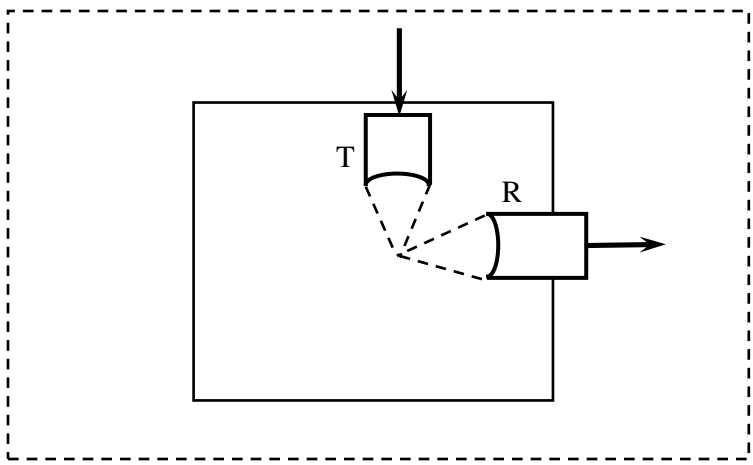

Figure 3.3 Scattering set-up

As shown in Figure 3.3, an acoustic arrangement with two transducers (transmitter and receiver) was employed in a plexiglas tank. All transducers were single element spherically focused transducers with a diameter of 0.0127 m. and a focal length around 0.03048 m. One transducer with a bandwidth of 85.061 % and a center frequency of 5 MHz was used as the transmitter (T in Fig. 3.3) for insonation at a frequency of 6.0 MHz. The 2nd transducer with a bandwidth of 80.687 % and a center frequency of 2.25 MHz was used as the receiver (R in Fig. 3.3). The transmit transducer was positioned confocally at right angles to the receiving transducer. Since contrast microbubbles are much smaller than the acoustic wavelength and undergo volume pulsation in an

ultrasound field, scattered signals received at 90° should be very similar to the backscattered echoes (Shi et al., 2000). The advantage of this measurement system is its high spatial resolution; this is because the scattered signals only come from the microbubbles in the small overlapping confocal region of the transmitting and receiving transducers.

A function generator and a power amplifier were used to produce a continuous sine wave, fed into the transmitting transducer. The signal was received by the receiving transducer, amplified by the pulser-receiver and fed into an oscilloscope and a computer. For each measurement, 64 sequences of signals were averaged in the oscilloscope and then transferred to a PC via an IEEE-488 (GPIB) interface for further analysis. The data transfer was controlled using Labview®. Matlab® was used for post-processing of the data. A 0.4 mm needle hydrophone was used to measure the acoustic pressure of excitation. All scattering measurements were carried out at room temperature (around 25° C). Distilled water was utilized as the carrying and propagation medium. Contrast agent used in these experiments was Definity. Definity microbubbles were prepared by shaking the suspension in a Vial-Mix™ for 45 s according to manufacturer's recommendations. The bubble suspension was then injected into water 2 min after preparation. Excitation was started 1 min after injection. A magnetic stirrer was used to produce a homogeneous solution containing microbubbles.

3.3 Method to determine the parameters of the shell

In chapter 2 we describe bubble shell parameters as the unknowns in the bubble dynamics equation. They are determined by comparing the experimentally

measured attenuation and the model prediction. The measured attenuation $\alpha^{meas}(\omega)$ over a range of frequencies ω is used to define an error $Er(\gamma, \kappa^s)$ or $Er(\gamma_0, E^s, \kappa^s)$:

$$Er(\gamma, \kappa^s, \cdots) = \sum_i \left[\alpha(\omega_i) - \alpha^{meas}(\omega_i) \right]^2 \tag{3.3}$$

where $\alpha(\omega_i)$ is the attenuation which is obtained numerically as mentioned in chapter 2, and the calculation is based on Eq. (2.23). The error is minimized to obtain the bubble parameters. MATLAB is used to execute the error minimization. We find the characteristic shell properties both for the viscous and viscoelastic models (chapter 4).

Chapter 4

RESULTS AND DISCUSSION

4.1 Suitability of broadband attenuation for characterization

The experiments were performed at a concentration of 40 µl of Definity in 1 l of Isoton-II and repeated four times. In Figure 4.1, we show the received signal with and without Definity microbubbles from a typical experiment. The presence of microbubbles clearly attenuates the transmitted pulse. In Figure 4.2 FFT (Fast Fourier Transform) of the time domain signals (Figure 4.1) displays the frequency content.

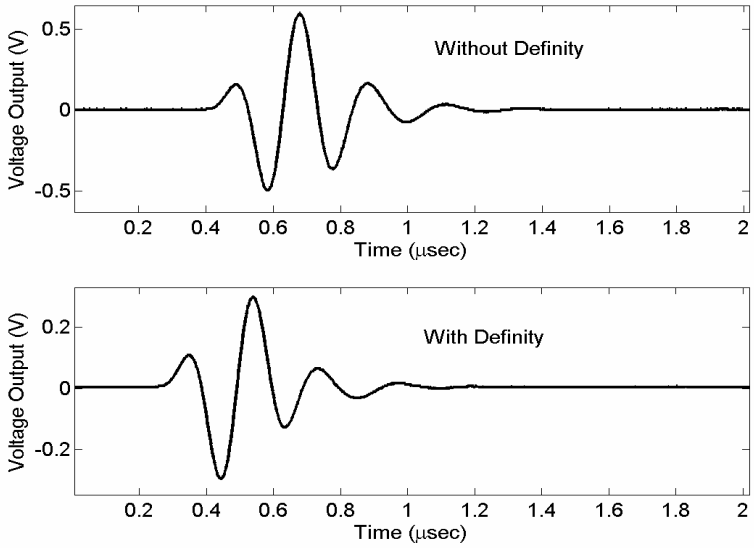

Figure 4.1 Signal received by the transducer (center frequency 5MHz) with and without Definity at a concentration of 40 µl/l in time domain, pressure-amplitude .67 MPa.

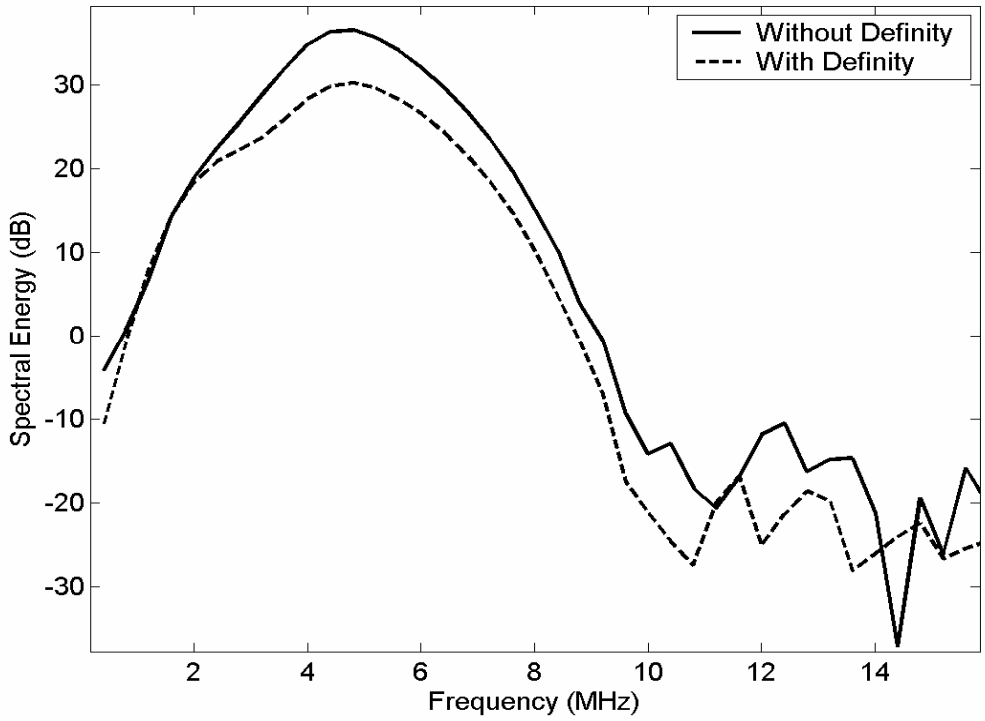

Figure 4.2 Frequency spectrum of the signal in Figure 4.1

4.1.1 Dependence of attenuation on transducer with different center frequencies

We investigated the dependence of attenuation on transducers with different center frequencies. Figure 4.3 shows the frequency spectra in the absence of bubbles for three transducers. Corresponding attenuation data obtained with Definity are plotted in Figure 4.4. The peak negative excitation pressure was 0.1 MPa. The attenuations measured with different transducers match with each other in the overlap region, indicating that the computed attenuation is independent of the transducer as well as the center frequency of the excitation pulse. Using three transducers, we obtained the attenuation due to contrast microbubbles in the frequency range of 2-6.5 MHz.

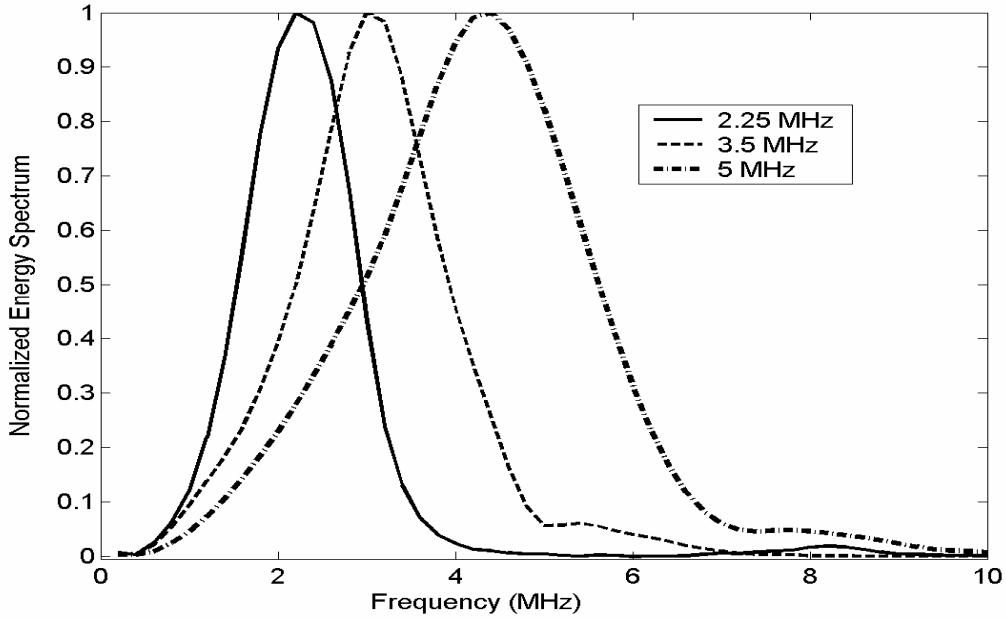

Figure 4.3 Normalized broadband signal sent by the pulser receiver to transducers.

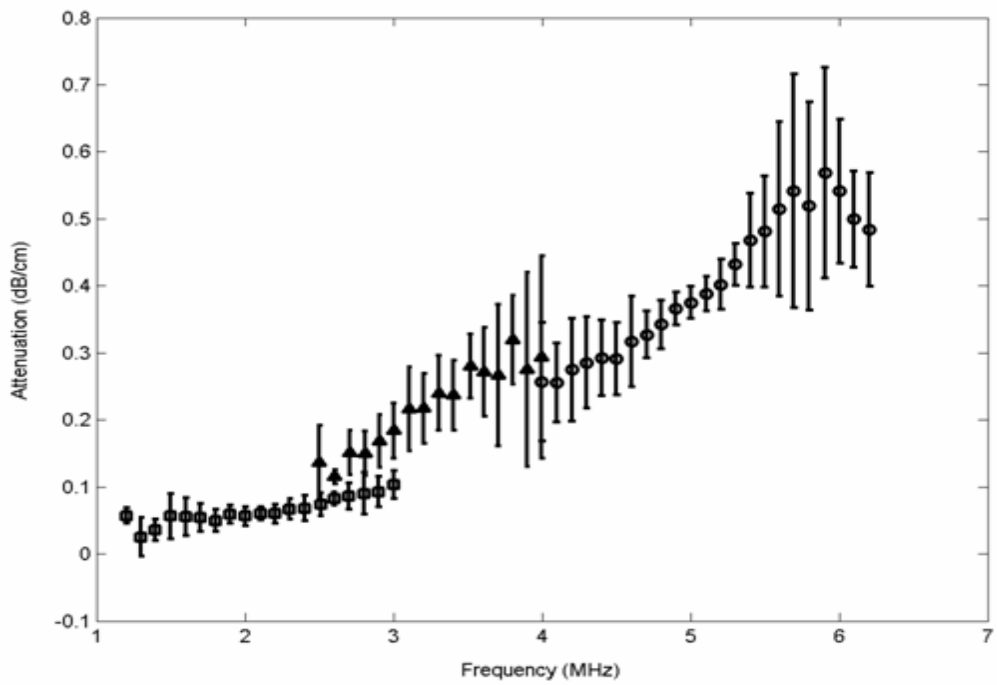

Figure 4.4 Attenuation measured by three transducers with center frequencies of 2.25 (square), 3.5 (triangle) and 5 (circle) MHz at .1 MPa, PRF was 100 Hz and Definity concentration was 40µl/l.

The spectrum shows a continuous increase with frequency with a slight peak at ~6 MHz and is a characteristic of the contrast agent, rather than of the excitation or the transducer center frequencies (2.25, 3.5 and 5 MHz). Chen et al (2002) found that the attenuation as

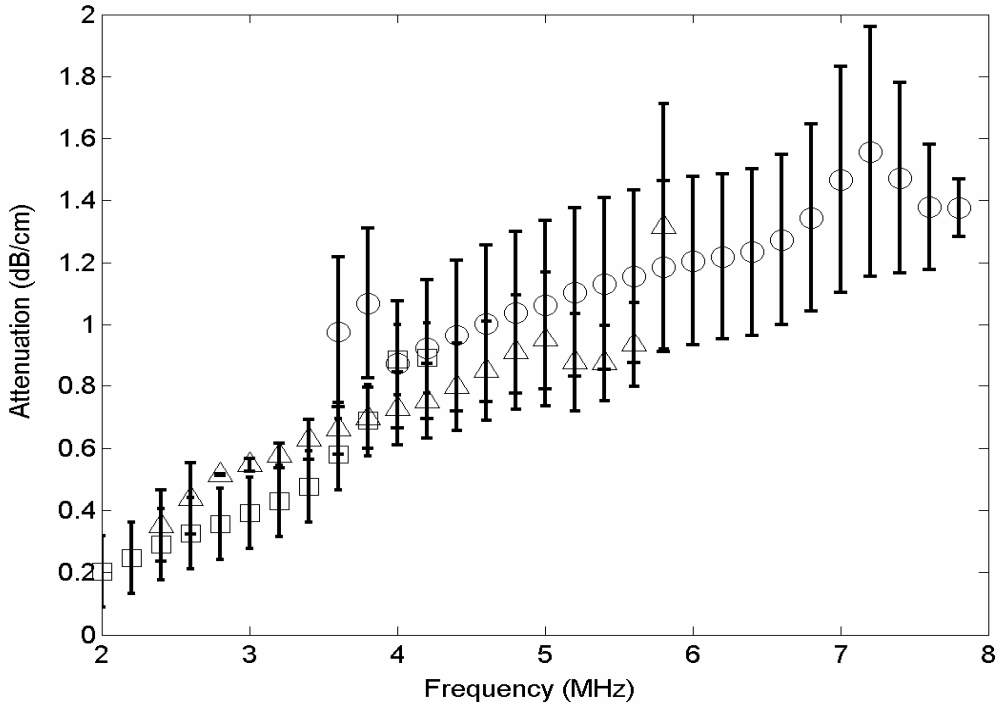

Figure 4.5 Attenuation measured by three transducers with central frequencies of 2.25 (square), 3.5 (triangle) and 5 (circle) MHz. at 0.67 MPa, PRF was 100 Hz and Definity concentration was 40µl/l.

a function of frequency (Figure 3 in Chen et al. 2002) measured with narrow-band incident pulses decreased steadily with increasing frequency in the range 1-5 MHz. Definity microbubbles are small (~1 micron radius). For a free bubble, the resonance frequency and radius are related by an empirical relation $f_0 = 3.25/r$, where r is the bubble radius in µm and f_0 is the resonance frequency in MHz (Leighton, 1994). For the size of Definity the corresponding free-bubble resonance frequency is ~3.25 MHz. The lipid encapsulation-induced elasticity further increases the resonance frequency.

Therefore, one would expect the attenuation to increase with frequency for the range of 1-3.25 MHz and beyond, as is indeed observed here (Figure 4.4). Similar observations were obtained even for higher pressure amplitude of 0.67 MPa (Figure 4.5). No bubble destruction took place under these conditions, as became evident from the constancy of attenuation data over a time interval of 10 minutes. Note that Chen et al. (2002), observed that using different center frequencies for excitation pulse (at a much lower amplitude of 0.15 MPa) resulted in very different attenuation, with peaks at those frequencies (Figure 7 in their paper). They argued that the nonlinear dynamics of suspended microbubbles are responsible for this behavior. We proceed to investigate this issue in further detail by explicitly computing attenuation at different excitation amplitudes.

4.1.2 Dependence of attenuation on excitation pressure amplitude

Effects of nonlinearity become significant with increasing excitation amplitude and one would expect that attenuation would be independent of the excitation amplitude below a critical value. We investigated the effect of excitation pressure amplitude by measuring attenuation at varying excitation amplitudes using the set-up in Figure 3.2 (Chapter 3). A transducer with center frequency of 5 MHz was used as a transmitter and one with 3.5 MHz, as a receiver. In Figure 4.6 and Figure 4.7 we compute attenuation (dB/cm) curves for increasing excitation amplitudes at a concentration of 40µl/l and 120 µl/l respectively.

.

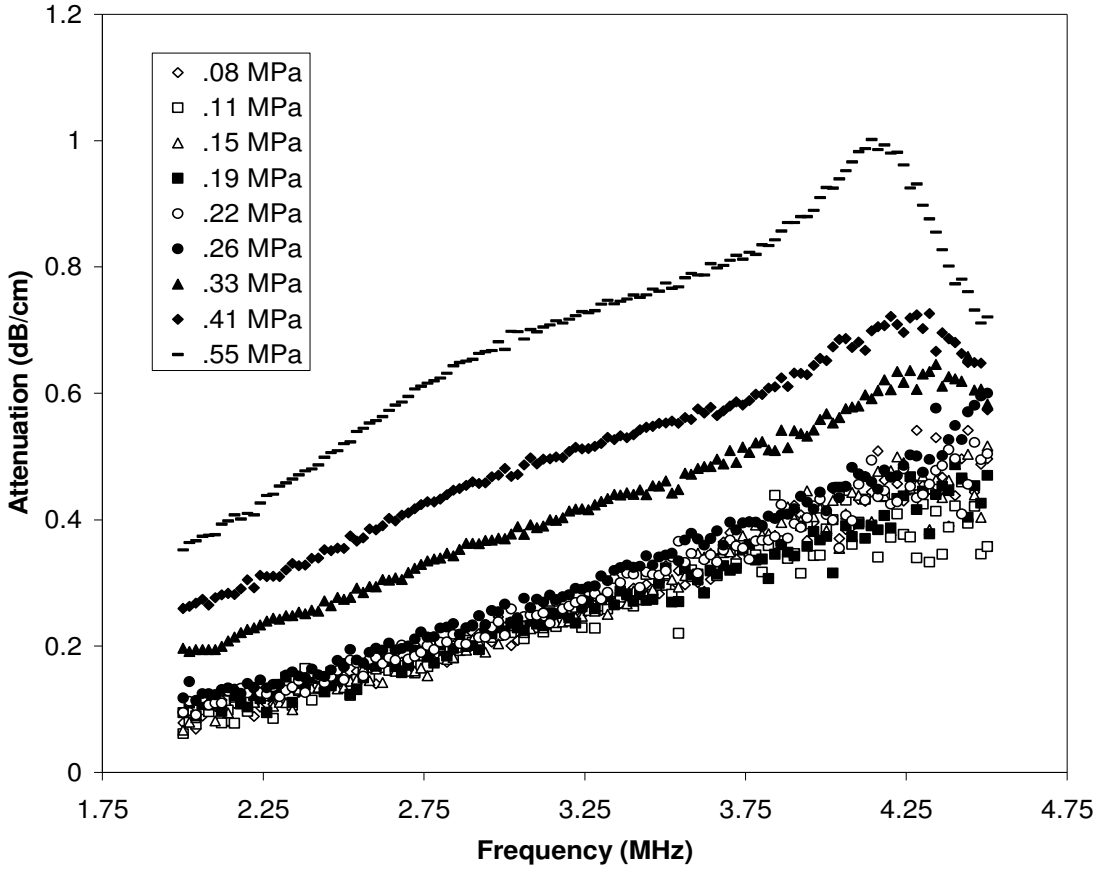

Figure 4.6 Variation of attenuation with incident pressure amplitude, concentration used was 40 μl/l.

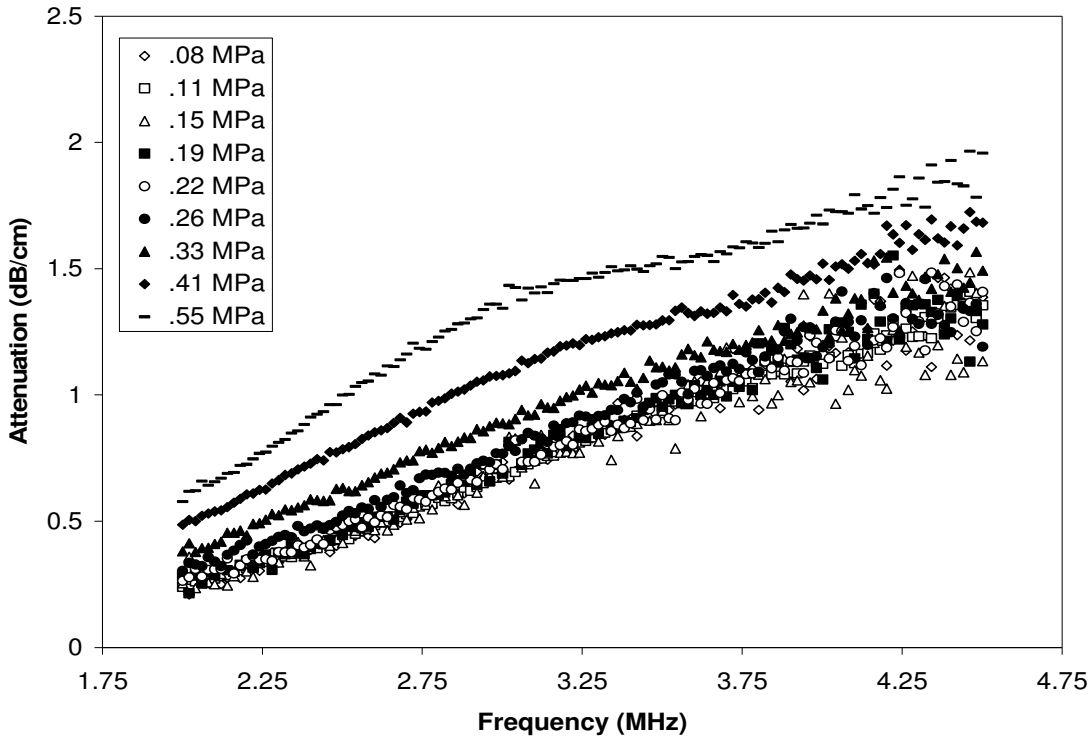

Figure 4.7 Variation of attenuation with incident pressure amplitude, concentration used was 120 µl/l.

We observe that the attenuation does not change with amplitude for excitation less than 0.26 MPa, but those above (top four curves) increase with amplitude. We conclude that nonlinearity sets in above the critical value of ~0.26 MPa. The linear propagation theory Eq. (3.2), are not valid above this critical value of pressure amplitude. Wu and Tong, (1997) and Zhang et al. (2000), observed increased nonlinearity in the medium with increased concentration, in that concentration may accentuate nonlinear wave propagation. However, Figure 4.7, for concentration of 120 µl/l, a three-fold increase, results in the same critical excitation amplitude (~0.26 MPa). Note that Chen et al. (2002), found the broad-band attenuation measurement to depend on the excitation amplitude for a far lower value of 30 KPa.

4.1.3 Linear dependence of attenuation with concentration of the microbubbles

Next, we investigate the effects of concentration at low pressure amplitude (.1 MPa). At lower concentration, bubble-bubble interactions can be neglected, as though the bubbles are acting in isolation, being excited only by the incident wave. Equations (2.23) and (3.2) describe such non interacting dynamics of the bubbly media, with attenuation varying linearly with concentration. At higher concentrations, interactions between bubbles and multiple scattering might play important roles. We measured attenuation with varying concentration using a broadband transducer with a center frequency of 5 MHz and excitation amplitude of 0.1 MPa. In Figure 4.8, attenuation corresponding to three different frequencies of 3, 4 and 5 MHz are plotted as a function of concentration. The figure shows that attenuation varies linearly with concentration in the entire range of concentration studied.

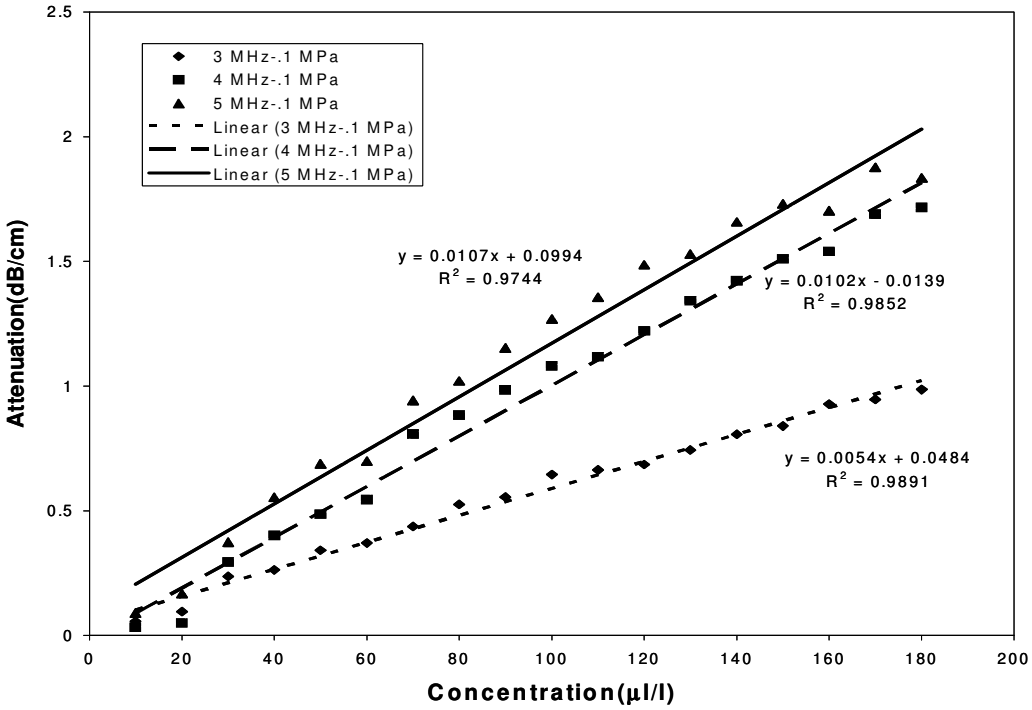

Figure 4.8 Variation of attenuation with concentration at excitation amplitude of 0.1MPa.

4.2 Characterization of ultrasound contrast agent Definity

We obtain the interfacial properties using the attenuation measurements and the linearized bubble dynamics equations Eq. (2.18) and (2.19). We use the mean size (2.2 μm diameter) of Definity® to calculate attenuation. We calculated the number of bubbles used for the concentration of 40 μl/l to be 4.8×10^{11} bubbles/m^3. Figure 4.4 shows the attenuation curve used to determine the properties. The theoretically calculated attenuation for the viscous model is fitted to the experimental data, Figure 4.9. The interfacial tension γ and the dilatational viscosity κ^s for Definity were determined to be

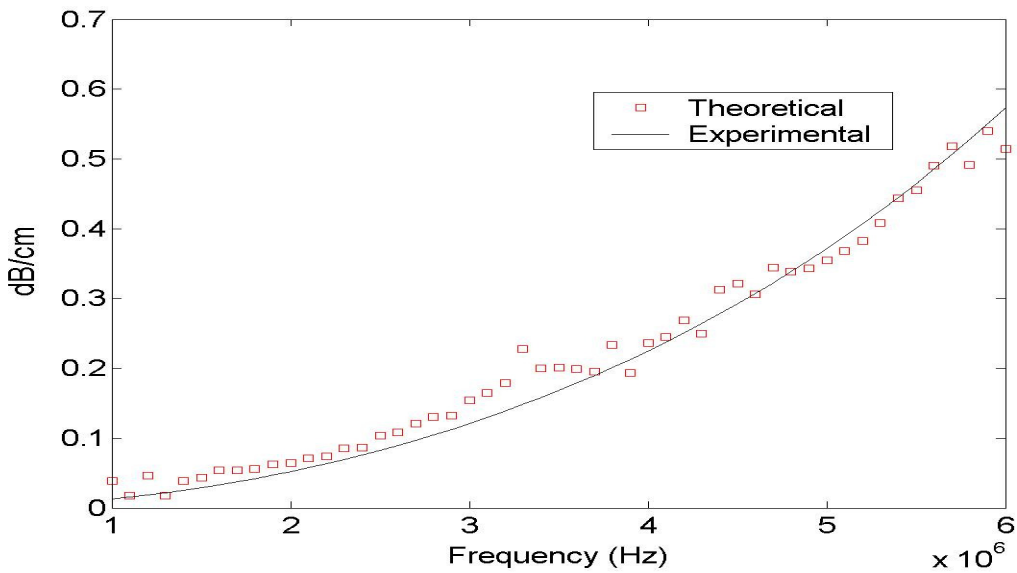

Figure 4.9 Determination of the interface (Newtonian viscous model) parameters corresponding to Definity® bubbles. Data corresponds to concentration of 40 μl/l of Definity® in Isoton-II

3.18 N/m, and 2.3 x 10^{-8} N-s/m respectively. The value of interfacial tension is large compared to the value in case of air-water interface. This was also observed for Optison (GE Health Care, Princeton, NJ) by Chatterjee and Sarkar (2003) and also for Sonazoid

(Amersham, Oslo, Norway) by Chatterjee et al. (2005). This is attributed to the fact that Newtonian rheology model adopted here does not have any interfacial elasticity term other than the surface tension. Surface tension results from the cohesive force between water molecules. Absorbed surface active materials such as lipids at dilute surface concentration weaken the cohesion reducing surface tension. However, the encapsulation with closely packed lipid configuration may give rise to cohesive interaction between lipid molecules. It will lead to an elastic resistance to area change of the encapsulation.

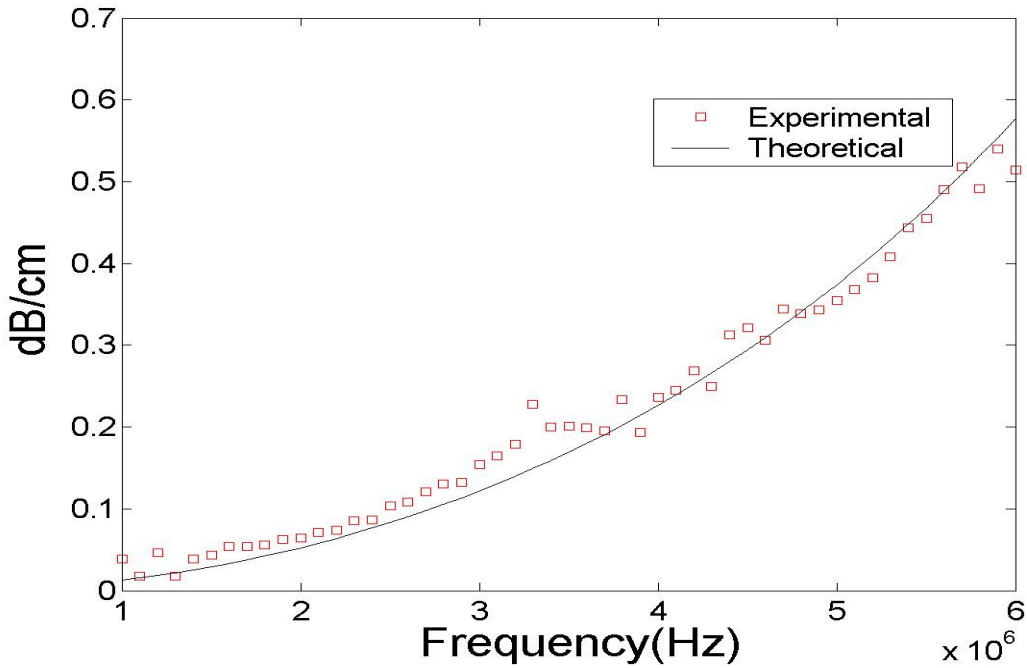

Figure 4.10 Determination of the interface (viscoelastic model) parameters corresponding to Definity® bubbles. Data corresponds to concentration of 40 µl/l of Definity® in Isoton-II.

The determined value of the surface tension should be interpreted as a model parameter representing the integrated effects of all "elastic effects" including the interfacial elasticity and surface tension. So, we considered the viscoelastic model

(constant elasticity) Eq. (2.12). The theoretically calculated attenuation data fitted to the experimental data for this model is shown in figure 4.10. With this model we get the surface tension γ_0 = 0.013 N/m, a value lower than that at the air-water interface, dilatational elasticity E^s =3.1905 N/m, κ^s= 2.3 x 10^{-8} N-s/m. The interfacial parameters obtained with the viscoelastic interfacial rheology (containing an explicit dilatational elasticity term) substantiates this explanation. Note that the surface dilatational viscosity κ^s remains the same in these two interface models, as it should if the property represents a physical nature of the encapsulation and not just a mathematical fitting constant. Surface tension γ in the viscous model is indeed a combination of surface tension and dilatational elasticity of the viscoelastic model—$\gamma \square \gamma_0 + E^s$.

4.3 Experimental investigation of destruction of microbubble contrast agents

Strong acoustic excitation leads to instability and destruction of microbubbles. Shi et al. (2000), have shown that for Optison bubbles, even before destruction, the attenuation spectrum changes with time. They also observed a shift in the peak towards lower frequency in suggesting an increase in bubble-size. It was attributed to the ingress of air into Optison bubbles and slow diffusion out of perfluorocarbon gas. However, the peak was observed to shift back in later times and the attenuation decreased. We measured attenuation for various excitation amplitudes and pulse repetition frequencies (PRF), and investigated bubble destruction as indicated by a decrease in attenuation with time. Under excitation, bubble destruction takes place in different ways, such as by slow outward diffusion of the gas, by rupture of the encapsulation and dissolution of the resulting free bubble, or through a catastrophic process of breaking up into smaller bubbles (Chomas et al., 2000). All of them will result

in decreased attenuation.

We performed attenuation measurement using excitations with varying PRFs and pressure amplitudes. Figure 4.11 shows the variation of normalized attenuation with time when bubbles are subjected to acoustic excitation with a PRF of 50 Hz under different pressure amplitudes. Figure 4.12 and 4.13 show the same plots for 100 and 200 Hz respectively. For the lowest pressure 0.78 MPa, we find that the attenuation level increases with time for all three PRFs. With increased excitation levels, the attenuation decreases with time, indicating a deterioration of the bubble population. We find that there is a threshold pressure, above which the measured attenuation shows a decrease with time. For all three PRFs, it is around 1.2 MPa, even though one would expect that the critical pressure for destruction would reduce with increasing PRF. Increasing the pressure amplitude beyond this critical value results in faster decrease of attenuation indicating faster rate of destruction.

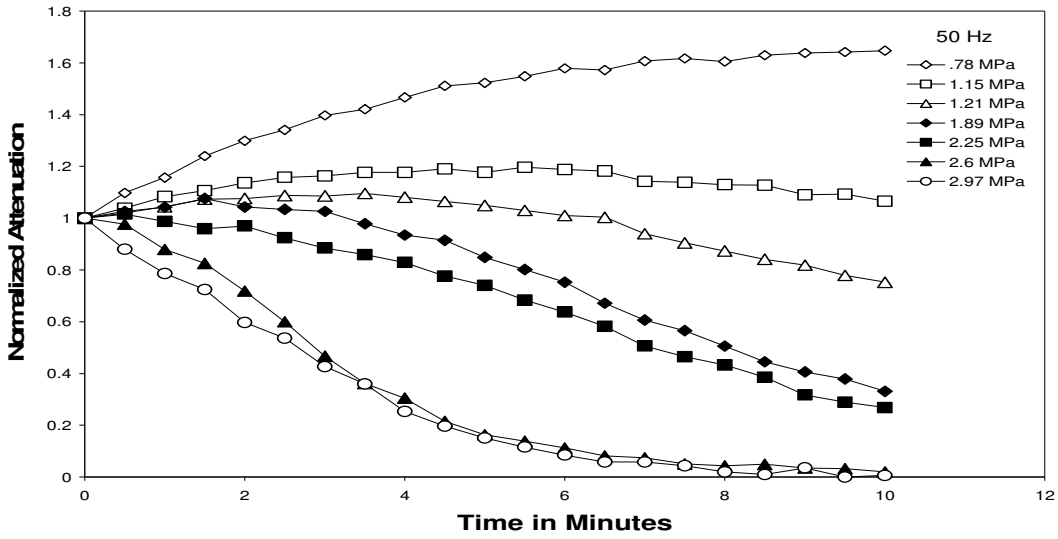

Figure 4.11 Variation of normalized attenuation with time under different acoustic pressure amplitudes for PRF of 50 Hz.

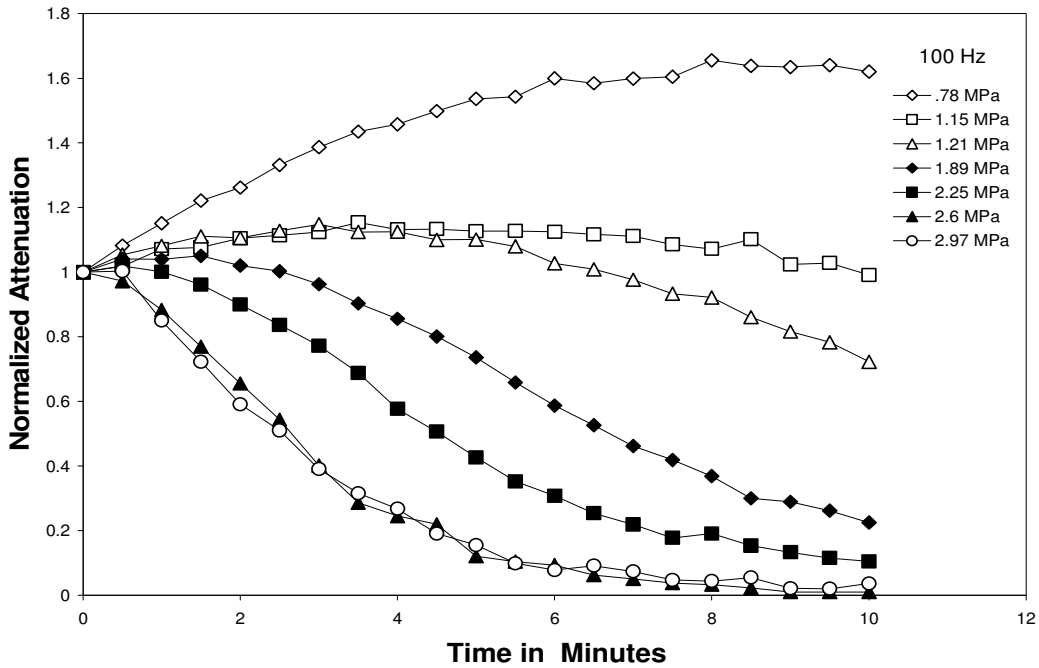

Figure 4.12 Variation of normalized attenuation with time under different acoustic pressure amplitudes for PRF of 100 Hz.

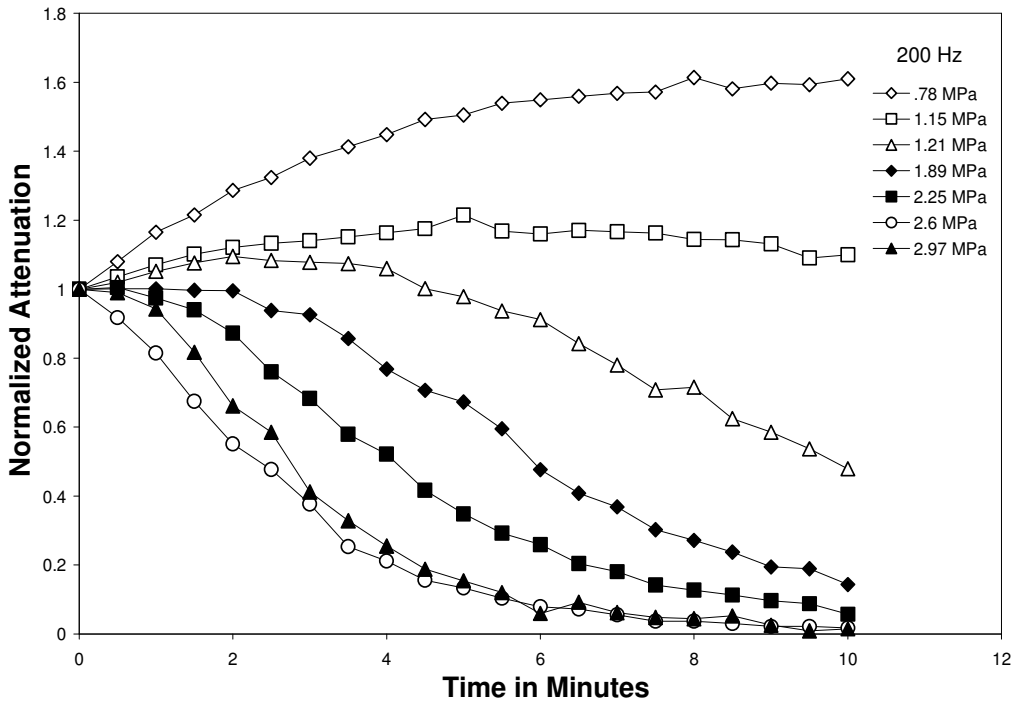

Figure 4.13 Variation of normalized attenuation with time under different acoustic pressure amplitudes for PRF of 200 Hz

At each PRF the rate of destruction is very slow at pressure values slightly above the critical pressure. For such cases, the primary mode of destruction is gas dissolution (Klibanov et al, 1998; Dayton et al, 1999; Chomas et al, 2000; Chomas et al, 2001). For the highest-pressure levels (2.6 and 2.97 MPa), the attenuation curves tend to overlap, suggesting that the destruction becomes independent of pressure values. The attenuation does not show much dependence on PRF as is evident from Figure 4.14 except for intermediate excitation levels. The excitation-independent attenuation decrease indicates a complete rupture of the encapsulation

Note that nonlinear emission from contrast agent under excitation has primarily been used in the literature as a signature of bubble fragmentation, and accordingly excitation thresholds were determined. Measuring scattered response with increasing pressure levels, Chen et al. (2003), determined an inertial cavitation threshold marked by sudden increase in frequency spectra between each pair of harmonics. They found fragmentation thresholds for Optison (0.13 MPa at 1.1 MHz, 0.48 MPa at 3.5 MHz), Sonazoid (0.15 MPa at 1.1 MHz, 0.58 MPa at 3.5 MHz), bisphere 0.2X (0.19 MPa at 1.1 MHz, 0.73 MPa at 3.5 MHz) and bisphere 0.7X (0.23 MPa at 1.1 MHz, 0.96 MPa at 3.5 MHz). Similarly, Sboros et al. (2004), found a maximum in second harmonic normalized back scatter for Definity at 0.5 MPa for 1.6 MHz driving frequency, and suggested bubble destruction above such pressure. Our experiment is performed under single cycle bursts form a 5 MHz transducer. The power delivered is lower at the higher frequency, which might explain our higher threshold value.

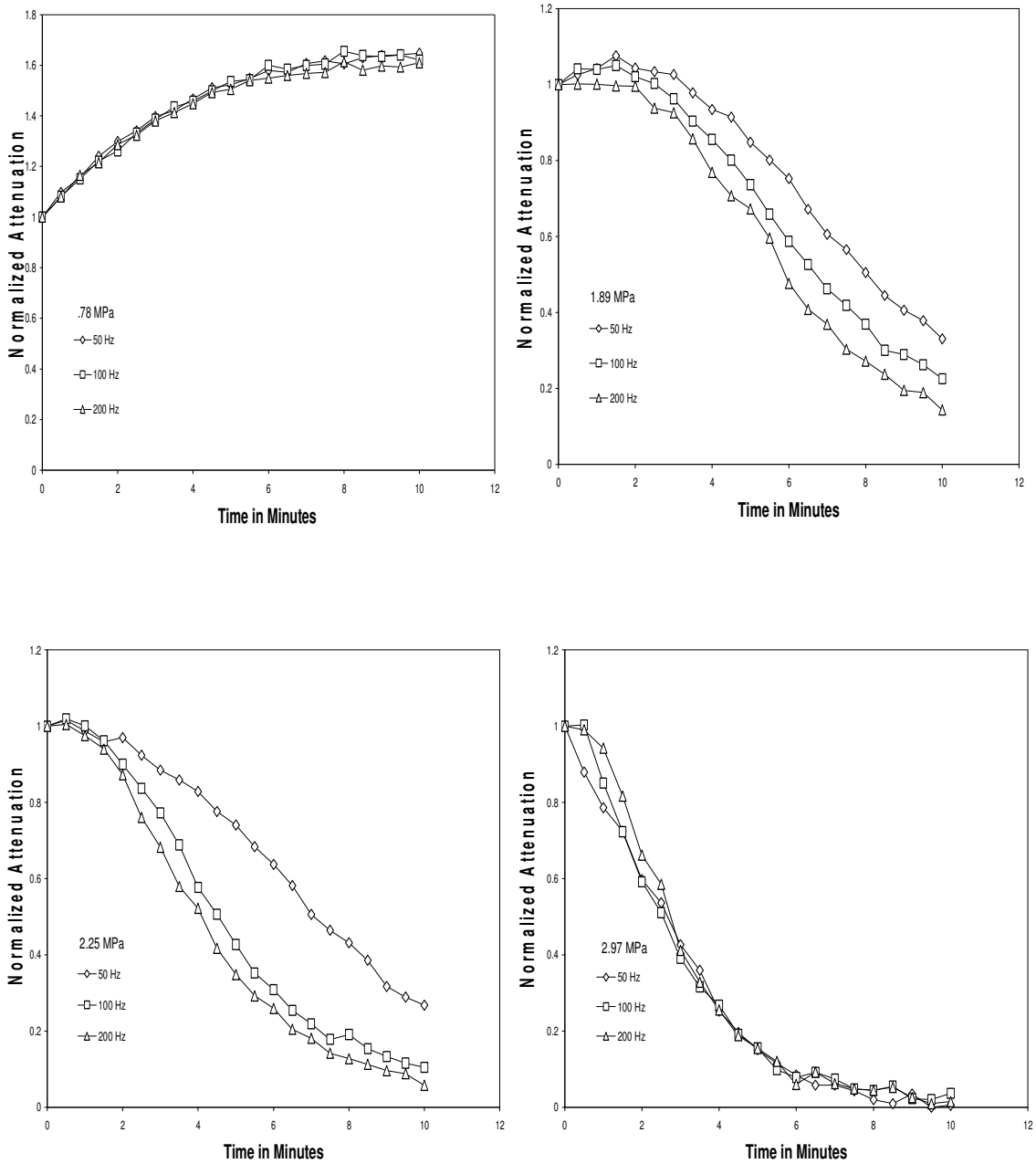

Figure 4.14 Normalized attenuation with time under different PRF at four different pressure amplitudes: (a) 0.78 MPa, (b) 1.89MPa, (c) 2.25 MPa and (d) 2.97 MPa

In Figures 4.11-4.13, we note that at lower pressure amplitudes, the attenuation tends to increase with time indicating a transient growth in bubble radius. The bubble oscillation at low levels of excitation results in increased permeability of the shell

and larger diffusion of gases. Definity bubbles are made with perfluorocarbon gas inside. Initially, more air will diffuse in than heavy, less soluble perfluorocarbon gas diffuses out as the time-scale of diffusion of these two gases are different (Kabalnov et al., 1998(I and II)). The increased bubble size will give rise to larger attenuation. Over a longer period of time, the process reverses, and the attenuation reduces. For 0.78 MPa, we do not see the eventual decrease in the time-scale of the experiment (10 minutes), but at slightly higher-pressure amplitude of 1.15 MPa we observe it. In fact, for many cases in the low to intermediate pressure amplitudes in Figures 4.11-4.13 display initial increase followed by the final decrease. Over longer period of time, the partial pressure of air inside the bubble reaches equilibrium with the dissolved air outside. The perfluorocarbon gas continues to slowly diffuse out and the bubble shrinks leading to reduced attenuation. Kabalnov et al. (1998), presented a model of multi-component microbubble dissolution that showed such an initial swelling of the microbubble over a very short time scale. However, the model did not account for permeability of the encapsulation, which would delay the process. A transient increase in bubble size due to gas diffusion was also reported by Guan and Matula (2004), where they determined the instantaneous bubble size by light scattering.

4.3.1 Modes of destruction and time-scale

Our study suggests that there are three distinct bubble behaviors—bubble growth at low pressures, excitation dependent destruction at intermediate pressures (higher than 1.2 MPa) and destruction independent of excitation at high pressures. Attenuation shows very weak dependence on the PRF. At higher pressure and later times the curves tend to overlap. At these pressure values the destruction is dominated by shell

rupture. The variation of normalized attenuation data with time is expressed by an exponential curve:

$$A(t) = A(0)\exp(-mt). \tag{4.1}$$

Here m, the decay constant, is a function of the intensity of excitation ($\sim P_A^2$) and the PRF. We obtained the decay constant (m) by fitting an exponential to the data set in Figure 4.11-4.13 taking only the descending part of the curves. Table 4.1 shows the values of m under different excitation pressures and PRFs. m increases with P_A. At the PRF of 200 Hz the destruction becomes independent of pressure above 2.25 MPa. The variation of m with it is shown in Figure 4.15 for different PRFs. m varies as $P_A^{1.8}$, $P_A^{2.0}$ and $P_A^{1.4}$ for PRF of 50, 100 and 200 Hz respectively. It should be noted that from a simple total energy consideration, one would expect m to be a function of $P_A^2 * PRF$.

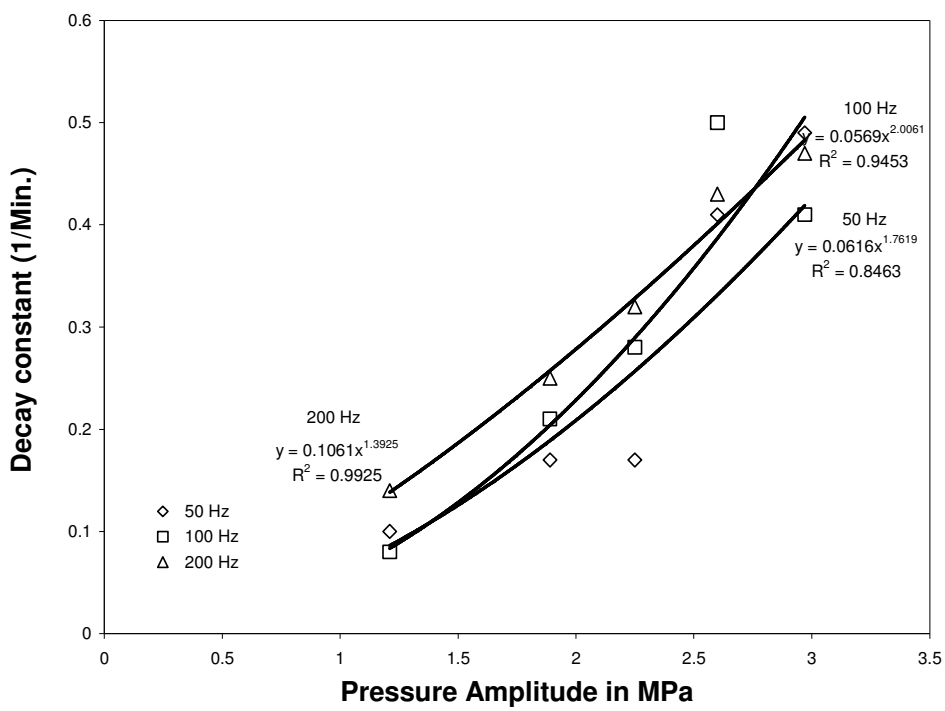

Figure 4.15 Variation of decay constant with pressure amplitudes P_A for varying PRFs.

However, note that the destruction is a combined effect of gas diffusion and shell rupture at larger pressure values and not just the total acoustic energy delivered that might explain the deviation.

Table 4.1: Values of decay constant *m* (min^{-1}) for different pressure amplitudes and PRFs.

Pressure in MPa	50 Hz	100 Hz	200 Hz
1.21	0.1	0.08	0.14
1.89	0.17	0.21	0.25
2.25	0.17	0.28	0.32
2.6	0.41	0.50	0.43
2.97	0.49	0.41	0.47

4.4 Scattering of ultrasound by microbubble contrast agents

4.4.1 Scattering from Definity® microbubble

We measure scattering of ultrasound in a solution of Definity at different pressure amplitudes, and investigate fundamental (Figure 4.16) and subharmonic (Figure 4.17) scattered responses. The fundamental response increases with exciting acoustic pressure for lower pressures as expected. The saturation in fundamental response is due to the nonlinear energy transfer into other frequencies at higher excitations. It might also be due to bubble destruction taking place at such high pressure amplitudes.

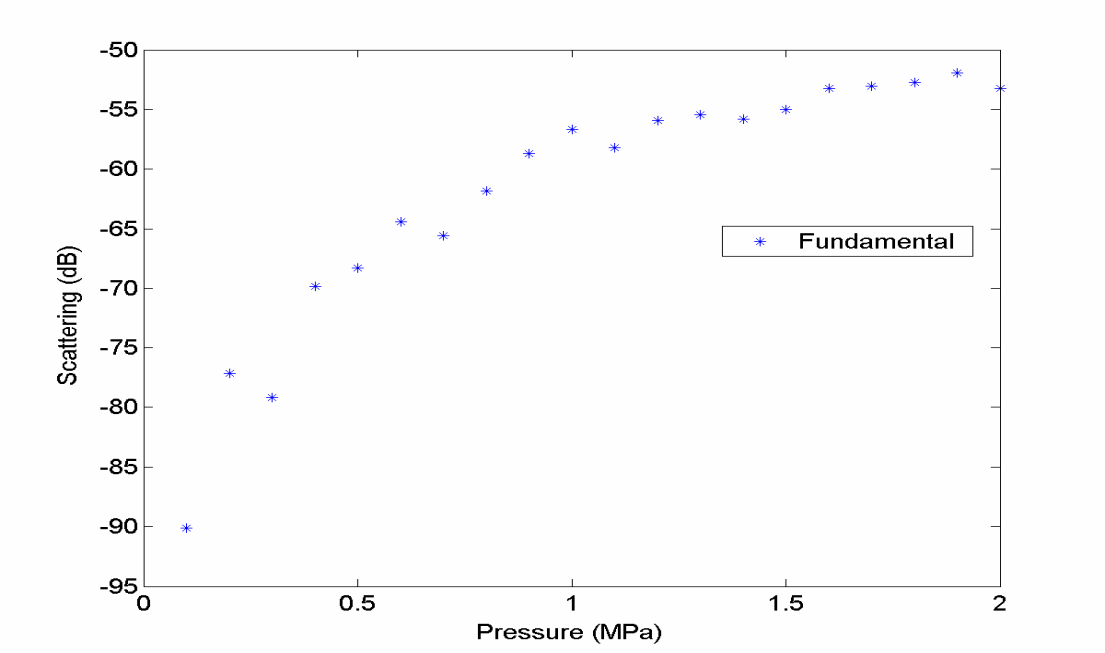

Figure 4.16 Scattered Fundamental response plotted with the pressure amplitude of excitation, 6 MHz driving frequency.

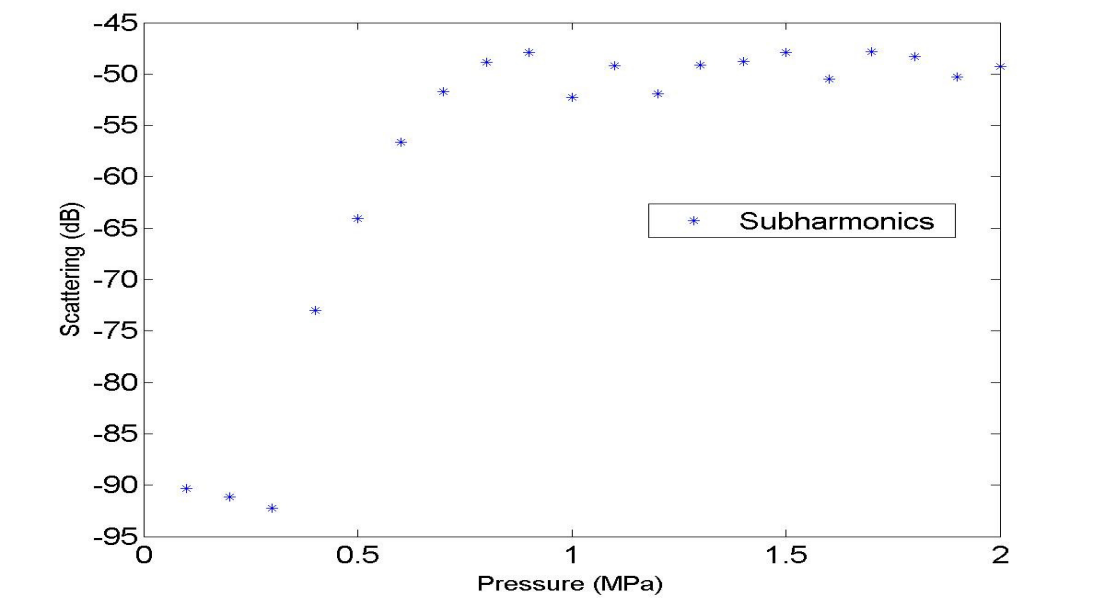

Figure 4.17 Scattered Subharmonic response plotted with the pressure amplitude of exciatation, 6 MHz driving frequency.

Figure 4.17 shows that a subharmonic response roughly has three different regimes with increasing pressure amplitudes — no significant subharmonic response, then its rapid growth and saturation. For sufficiently low level of excitation, the subharmonic component is insignificant (near the noise level, e.g. for pressures upto 0.3 MPa at 6 MHz insonation). At intermediate pressures (0.3-0.8 MPa), the subharmonic response increases rapidly, and usually has amplitudes much above the background noise. As the acoustic pressure increases further (e.g. 0.8 MPa for 6 MHz insonation), the growth of the subharmonic component saturates. Rapid growth and saturation trends were also observed in the case of Optison (Shi et al., 1999). At high pressure amplitudes, the noise level is substantially high, and the signal-to-noise ratio is greatly reduced and possibly bubbles are getting destroyed, leading to a saturation of the subharmonic. The experimental results now need to be compared with the simulated scattering results to validate the bubble dynamic model.

4.4.2 Scattering from Sonazoid: comparison between experiments and model

Validation of the models was done using the Sonazoid experimental data available in the literature (Chatterjee et al., 2005). In the theoretical simulation we have used a 64 cycle Gaussian pulse, with pulse length of 50 micro-secs, 2 MHz driving frequency. We calculated the scattered pressure by using Eq. (2.24). The scattered pressure from Eq. (2.24) is operated with a FFT to obtain the results in a frequency domain for various harmonics the simulation is scaled to match the experimental data for the lowest pressure level. The model parameters were determined using attenuation with a linearized equation valid only for small oscillations (Chapter 2 and 4). The underlying

assumption is that the determined material properties retain their validity for different types of experiments (scattering or attenuation), and also remain constant in a range of magnitude of oscillation (they may change for too large an oscillation, e.g. shear rate dependent interface viscosity/elasticity and interfacial tension).

Subharmonics are plotted in dB for various pressures in Figure 4.18, using both the viscous and the viscoelastic model. For the viscous model the scattered pressure pressure keeps on growing with the increasing excitation pressure, due to the

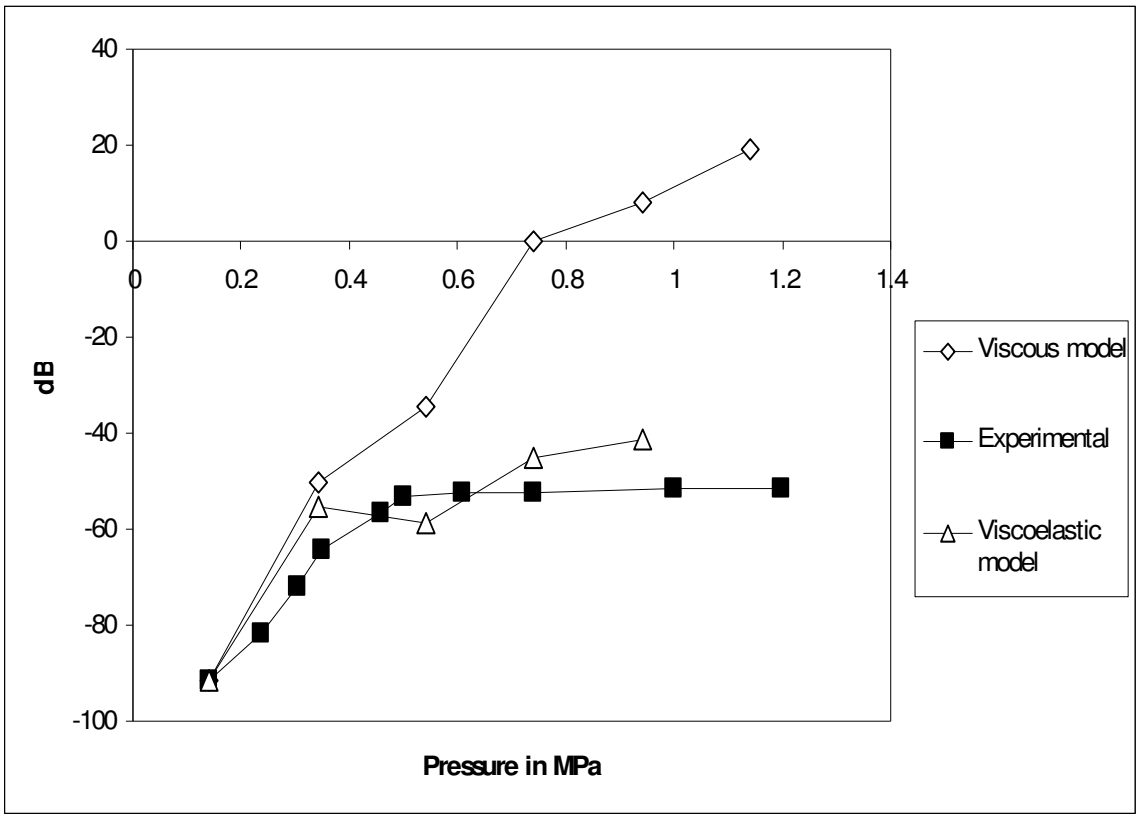

Figure 4.18 Plot for the subharmonics in dB with varying pressure amplitude of excitation

fact that in the model the shell properties do not change with the increasing pressure. The shell remains intact all the time and thus the model cannot account for the bubble

destruction, thus resulting in no reduction or saturation in the scattered pressure. In the experimental data we do observe the saturation in the subhramonics at higher pressure amplitudes which can be attributed to bubble destruction. Figure 4.18 also plots the subharmonics for the viscoelastic model. Clearly, if we compare the results for the viscous and the viscoelastic models, the viscoelastic model works better. As we discussed earlier, there is a need for the viscoelastic model, and we see that the results of this model compare well with the experimental results.

4.5 Model of growth and dissolution of contrast microbubbles

When ultrasound contrast agents are subjected to low intensity ultrasound repeatedly, their shell starts forming defects. Depending upon the diffusivity of the gas in the medium containing the bubble and the gas inside the bubble, the bubble can actually grow in size for a particular period of time. After growing to its maximum size the bubble starts to dissolve. The rate of the bubble growth and dissolution depends on many factors. We discuss this in detail in the following sections. All the sections considered here are for the steady state diffusion of gases from a shelled microbubble, without any ultrasound excitation.

4.5.1 Effect of the variation of the mole fraction of the osmotic agent and shell permeability

The variation of R/R_o with time for varying X_F is shown in the Figure 4.19. As the mole fraction of the osmotic agent (OFP) increases, both maximum radius and dissolution time increase (Kabalnov et al., 1998). The outside medium is saturated

with air, and devoid of the OFP. This initial growth is due to the sudden ingression of air into the bubble (Shi et al., 2000), the coefficient of the diffusivity of air

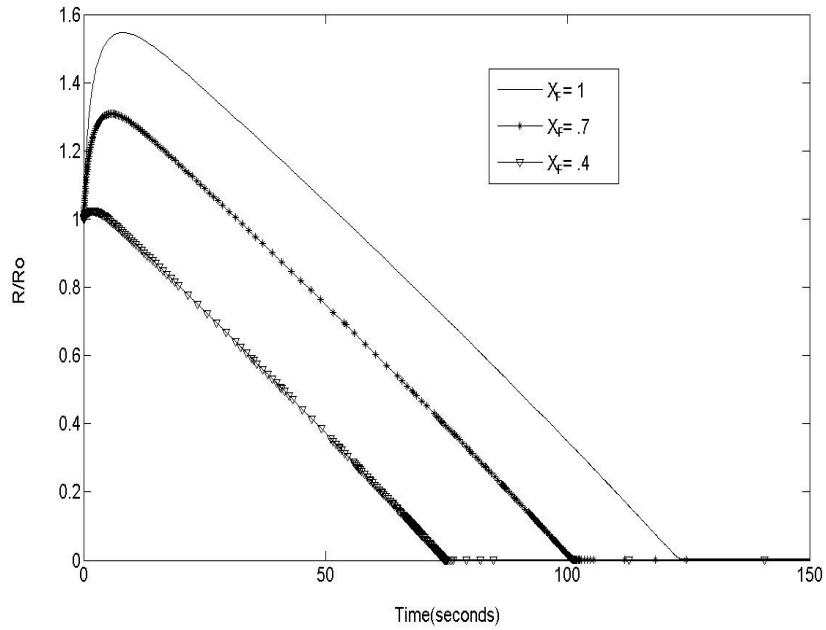

Figure 4.19 Permeable shell, variation of R/R_o with time for varying mole fractions of OFP, $f = 1$.

being higher than OFP. Figure 4.20 shows the variation of R/R_o with time for bubble with no shell, permeable and less permeable shell, $X_F = 1$. The permeability of the permeable shell is 0.001$\left(k_g/l\right)$. The parametric values for k_A= 2e-9 m^2/s, k_F= 7.45e-10 m^2/s, l= 15e-9 m. With decreased permeability of the shell the life time of the bubble is increased. We see that the time of dissolution of the bubble increases from ~10 seconds for the free bubble, to a few minutes for the less permeable shelled bubble. The bubble with no shell can be thought as the shell with infinite permeability. The thickness of the shell can be increased to reduce the permeability (inversely proportional to shell thickness), and hence increase the life time of a bubble.

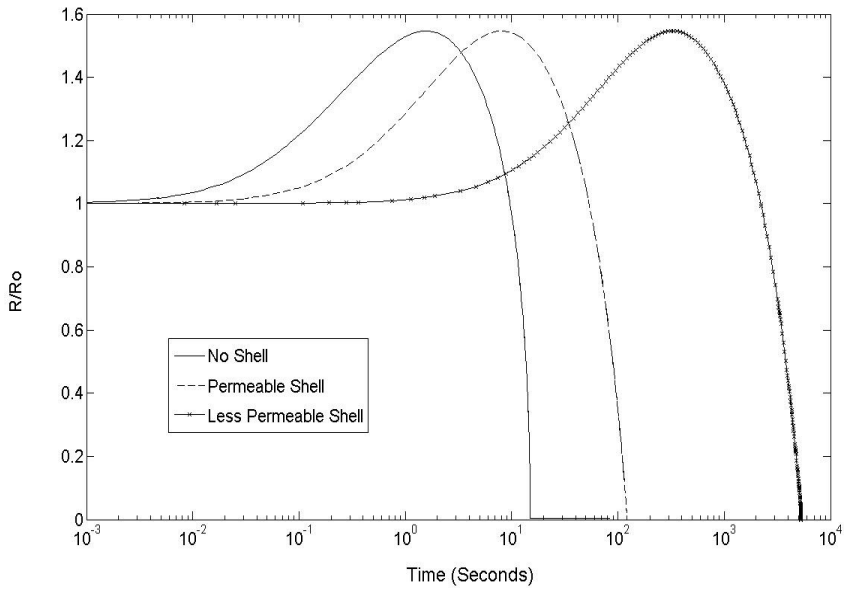

Figure 4.20 Variation of R/R_o with time for different shells- no shell, permeable shell- $.001\left(k_g/l\right)$, less permeable shell-$.00002\left(k_g/l\right)$.

4.5.2 Surface tension effects

Surface tension causes the dissolution of the bubble. In Figure 4.21 we plot R/R_o with time for varying surface tension. The ratio of R/R_o increases and then reaches a steady value for $\gamma = 0$. It reaches a steady value as a result of inside pressure equalizing the atmospheric pressure. When surface tension is non zero in the pressure balance Eq. (2.36), the quantity R/R_o decreases at the later time stages and finally reaches zero. This excess pressure due to surface tension drives the dissolution. The excess pressure increases as the bubble radius decreases.

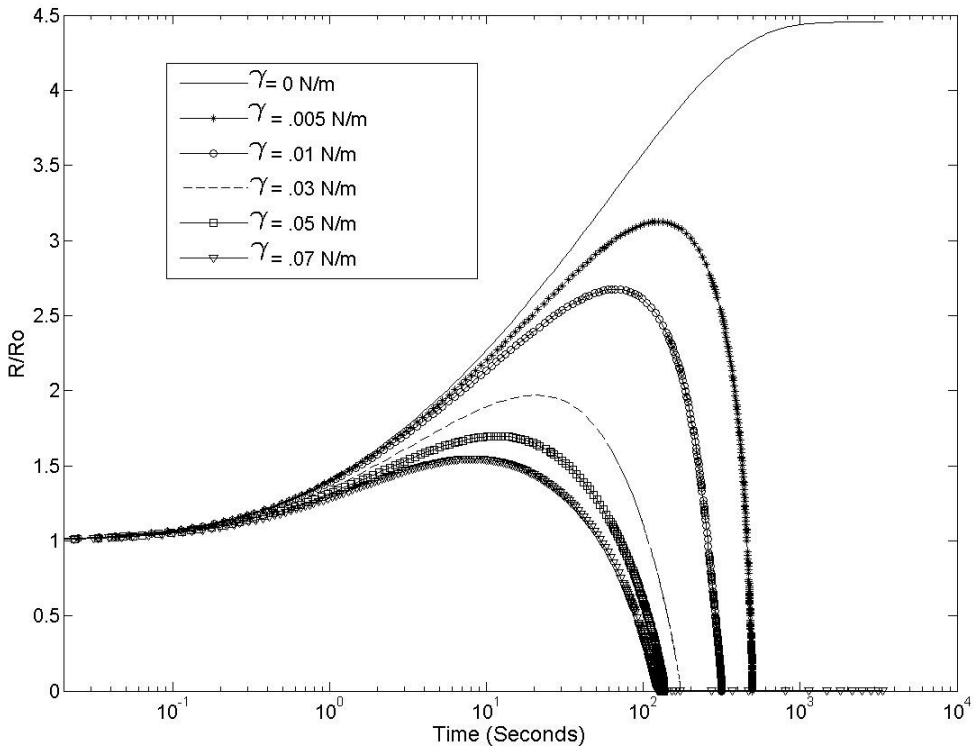

Figure 4.21 Variation of R/R_o with time for varying γ, for bubble with permeable shell, $X_F = 1$, $f = 1$.

4.5.3 Undersatuaration effects

We considered the dissolution of the bubble where the liquid outside (water) is undersaturated. We have assumed that there is only air in the bulk (water). Figure 4.22 shows the plot of R/R_o with time for varying f. We considered a permeable shell with zero surface tension, $X_F = 1$. When the water is saturated with air the bubble does not dissolve. When the outside liquid is undersaturated the bubble tends to dissolve

in spite of the surface tension being zero. Saturation level in the liquid in which the bubble exists forms the driving force for the dissolution of the bubble. These microbubbles are injected into the blood stream where the concentration of the metabolic gases changes continuously, which will affect the flow of gases in and out of the bubble (Vanliew et al., 1997).

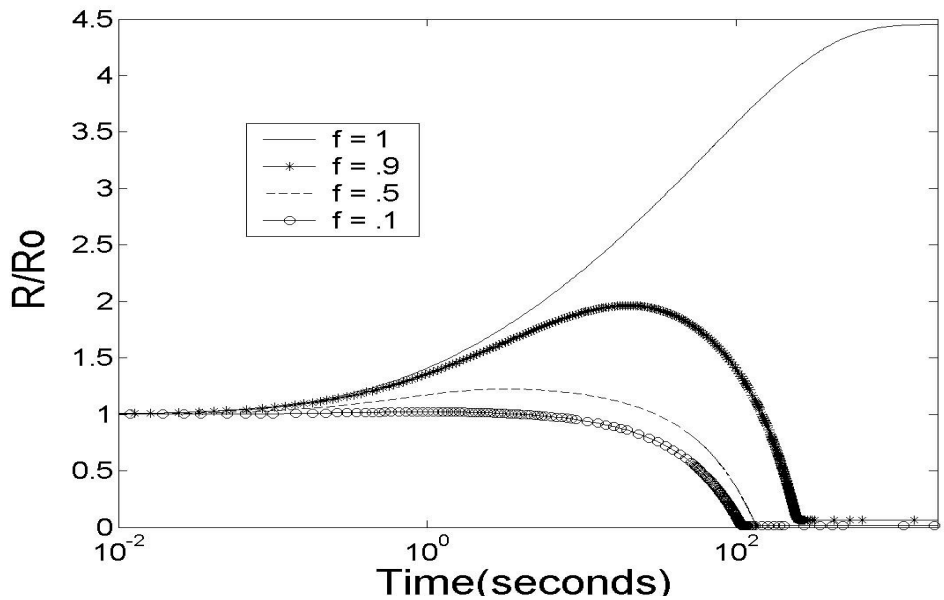

Figure 4.22 Permeable shell , R/R_o plotted with time for varying f , $\gamma = 0 N/m$.

4.5.4 Elasticity effects

We consider the elastic shell with elasticity E^S and the equilibrium radius to be the initial radius R_o. Eq. (2.42) is the pressure balance after inclusion of elasticity into the model (Chatterjee et al., 2005). Eq. (2.37), (2.38) and (2.44) are solved simultaneously for ρ using the initial conditions Eq. (2.36). It is interesting to note that if surface tension is set to zero in Eq. (2.42), the minimum value attained for the ratio R/R_o is 1 (Figure 4.23). At $R/R_o = 1$, the elasticity term vanishes in the Eq. (2.42) and

the inside pressure becomes equal to the atmospheric pressure. There is no extra pressure inside the bubble to drive the gases out of the bubble. Elasticity affects the growth of the bubble. If we reduce the elasticity, the bubble grows more (Figure 4.23), which is expected.

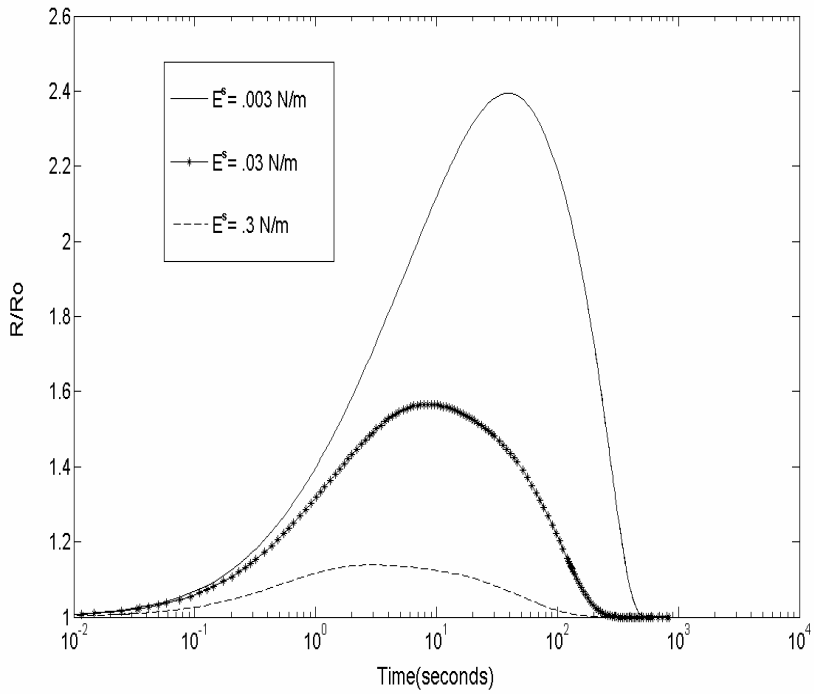

Fig. 4.23 R/R_o plotted with time for varying E^s, $\gamma = 0 N/m$, permeable shell, $f = 1$.

We considered the effects of elasticity for non zero value of surface tension. In Figure 4.24 we have plotted R/R_o with time for varying elasticity, $\gamma = .07 N/m$. Note that in Figure 4.23, R/R_o does not go below 1 as there is no γ to make inside pressure higher. In comparison, in Figure 4.24 we have a non zero value for γ which allows the inside pressure to be still higher than the outside pressure for $R/R_o =$ 1, giving R/R_o < 1 at later times. The bubble dissolves if the stress developed due to surface tension dominates the stress developed due to elasticity (E^s =.003 N/m, E^s =.03

N/m in Figure 4.24). If it is opposite, then the bubble will not dissolve as can be seen for the case where E^s =.3 N/m in Figure 4.24. The elastic stress competes with the stress developed due to surface tension and plays a vital role in the growth and dissolution of the bubble. This is very important for designing the shell for these bubbles, to fulfill the specific medical requirement. Imaging demands the oscillation of the bubble which requires the elastic stresses to be less dominant, but also should not be so low, that the bubble dissolves quickly. For drug delivery and arteriogenesis, bubbles need to be destroyed in a relatively easier fashion. The elastic stress should not be too high, as it becomes difficult to dissolve the bubble. We require an optimum value of elasticity.

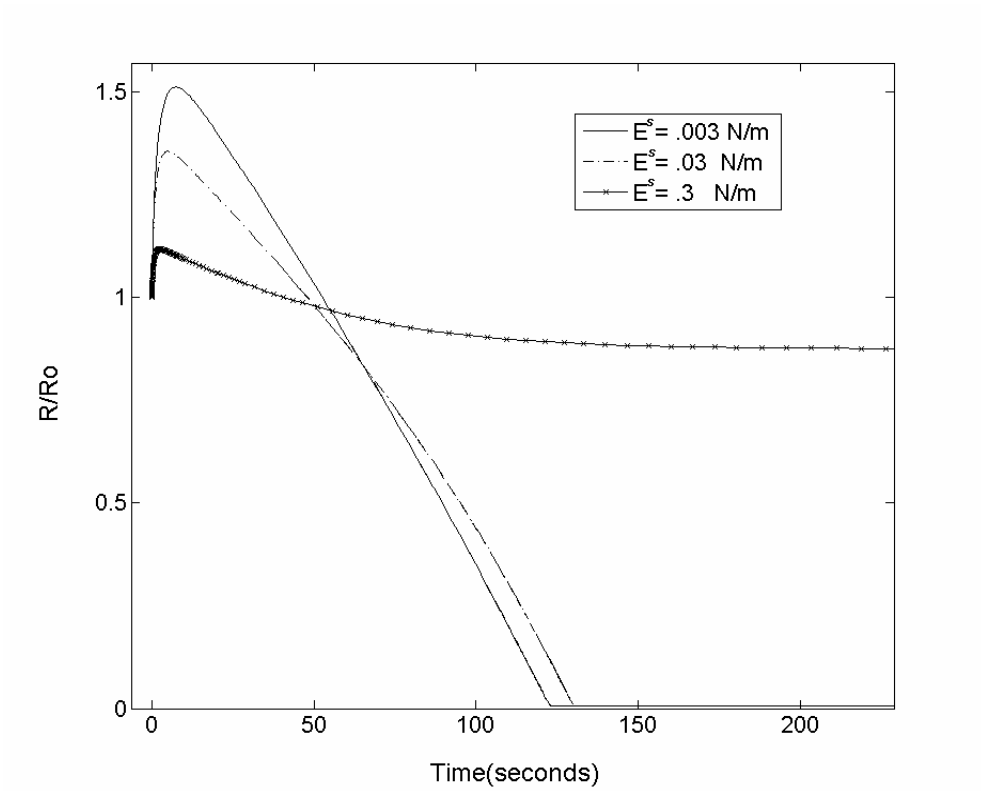

Fig.4.24 R/R_o plotted with time for varying E^s, $\gamma = .07 N/m$, permeable shell, $f = 1$

Chapter 5

CONCLUSIONS AND FURTHER RESEARCH

5.1 Final summary

In this thesis we have conducted experiments and numerical simulations to understand the performance of contrast agents. Chapter 2 presents relevant theory and modeling that provided a means to quantify and explain the experimental results. Chapter 2 describes the structure of the contrast agents, size distribution, their persistence, and different models used to describe their dynamics. It also explains the attenuation and the scattering theory used to characterize the microbubble shell and determine their behavior at higher pressure amplitudes respectively. Chapter 2 also describes the model developed for bubble growth and dissolution due to diffusion of the gases. Chapter 3 describes the experimental setups used for studying the attenuation and scattering by these contrast microbubbles when they are acoustically excited. It also describes the method to determine the shell properties of the microbubble. Chapter 4 presents and discusses the results.

5.2 Conclusions

5.2.1 Suitability of the broadband attenuation measurement for characterizing microbubbles

Attenuation of ultrasound through Definity measured with different transducers match in the overlap region for a concentration of 40 µl/l. Chen et al. (2002)

found it to depend on excitation pulse with amplitudes even in the low range of 0.03-0.15 MPa, and concentration -114 µl/l. However, we find that such is not the case; in fact the linear model of attenuation, as described by Eq. (2.23) and (3.2) becomes invalid only above a critical value of excitation amplitude, in that the computed attenuation becomes dependent on excitation amplitude. For Definity, the critical excitation amplitude at two concentrations of 40 µl/l and 120 µl/l considered is ~0.26 MPa, a value higher than that indicated by Chen et al. (2002). Chen et al. (2002) also found that the attenuation measured with narrow-band pulses decreased with frequency in the range of 1-3 MHz. Using the empirical relation between radius and resonance frequency, one would expect the attenuation to increase in the same range, as is observed in the current work. Their set-up does differ from the one adopted here. However, the underlying theory for analyzing the data is the same. The reason behind the discrepancy is not apparent at this point, and further investigation is warranted. We conclude that measurement of broadband attenuation can be used to characterize contrast microbubbles.

5.2.2 Model for characterizing the bubble shell

Here we presented two different rheologies for shelled bubble models—1) *viscous Newtonian* (surface tension γ, dilatational surface viscosity κ^s) and 2) *viscoelastic* (surface tension γ_0, surface dilatational viscosity κ^s, and surface dilatational elasticity E^s). The rheological properties for the models were determined by comparing predictions of a linearized dynamics with attenuation measured at small excitations. The characteristic rheological properties for Definity® are γ = 3.18 N/m, κ^s = 0.023 msP for the viscous model. The abnormally high value of the interfacial tension arises

from elastic effects due to the strong attraction between adsorbed materials at the interface. The lack of an explicit elastic term in the model leads to a lumping of all elastic effects in the surface tension term. This motivated us to use a viscoelastic model. The viscoelastic model results in κ^s = 0.023 msP, γ_0 = 0.013 N/m, a value indeed much lower than that (~0.07 N/m) at the air-water interface, and E^s = 3.1905 N/m. Furthermore, the unchanged value of the dilatational viscosity after the introduction of the new term (dilatational elasticity) is a welcome feature. A characteristic material parameter should not change when a different aspect (elastic as opposed to viscous) of the model is improved. So, in terms of quantification of the shell properties the viscoelastic model works better.

5.2.3 Destruction of contrast microbubbles studied experimentally

Investigation of destruction of contrast microbubbles under acoustic excitation taking the Definity microbubble as a test case is done. These are ~2.2 μm diameter bubbles stabilized by a lipid encapsulation. We measure attenuation of ultrasound through a solution of Definity as a function of time at various pressure amplitudes and PRFs. For smaller pressure amplitude (e.g. 0.78 MPa) we obtain an increase in attenuation with time, indicating bubble growth due to gas diffusion. There is a critical pressure level above which attenuation tends to decrease with time, indicating bubble dissolution. The critical pressure level is ~1.2 MPa for all three PRFs (50,100 and 200 Hz) considered here. The rate of destruction increases with increase in pressure amplitude, suggesting a slow mechanism of gas diffusion. In contrast, at very high pressures the process becomes independent of excitation conditions and the steep decay

indicates a faster destruction mode by shell rupture. The destruction shows only a weak dependence on PRF. We also fitted an exponential decay curve for the decay in attenuation. The decay constant *m* varies as ~ $P_A^{1.8}$, $P_A^{2.0}$ and $P_A^{1.4}$ for PRF of 50, 100 and 200 Hz respectively.

The ultrasound-mediated transient bubble growth below critical pressure would help achieve an enhanced scattering in an ultrasound activated contrast imaging. In this mode, a second activating pulse could be used to induce bubble growth shortly before the imaging pulse is sent to obtain enhanced scattering signals from activated contrast bubbles. The saturation in bubble breakup at higher-pressure amplitudes (decreased attenuation being independent of pressure amplitude) indicates that one need not use any higher strength for inducing destruction, which might cause damage to the surrounding tissue. Further *in vivo* research is needed to establish optimum operational ranges for different clinical applications.

5.2.4 Scattering by contrast microbubbles

Scattering by Definity and Sonazoid with varying amplitude of acoustic excitation has been studied. The fundamental scattered response grows for small values of excitations before slowing down at higher values. The measured subharmonic emission for Definity displayed rapid growth beyond a critical pressure amplitude (0.3 MPa) and then there is saturation in the scattered pressure values, which might be an indication of bubble destruction at these high pressure amplitudes. The experimental results were used to compare with the simulated results got from the bubble dynamics equation for Sonazoid in turn to validate the model.

5.2.5 Numerical study of growth and dissolution of contrast microbubbles

Ultrasound contrast agents have been used in the medical field for a long time now. Two factors, the growth and the dissolution, of these bubbles have been found to be very important for varied medical applications. Here we have modeled the bubble with a semi-permeable membrane around it. The bubble consists of two gases air and OFP. Increasing the mole fraction of the sparingly soluble gas inside the bubble (OFP), increases the growth and the dissolution time of these bubbles. Decreasing the shell permeability increases the life time of the bubble from few seconds to minutes, as a result of reduction in the free exchange of gases. Surface tension causes the dissolution of bubble. It becomes a very important factor in the design of the shell for bubbles. However the dissolution is also affected by the saturation level of the liquid outside the bubble. Undersaturation leads to dissolution of the bubble, even for the case where surface tension is zero. The most interesting part is the inclusion of the elasticity in the shell. Elasticity hinders the growth of the bubbles. Reducing the elasticity, helps the bubble to grow more. Elastic stresses compete with the stress due to surface tension. When the elastic stress dominates the bubble does not dissolve.

5.3 Further Research

Several aspects of ultrasound contrast agents warrants further research. One needs to investigate the agent destruction at 37^0C (body temperature). On the modeling side, development of a model that accounts for shell becoming permeable under excitation would lead to dynamic predictions of acoustic response from a changing

microbubble. We are currently investigating the two-frequency excitation of contrast microbubbles, where the excitation pulse is of higher pressure amplitude, which helps the bubble grow, and then the imaging pulse is sent at low pressure amplitude. This provides an efficient means of achieving enhanced image contrast, without risking possible tissue damage caused by high amplitude excitations.

BIBLIOGRAPHY

Borden, M. A., Longo, M. L. "*Dissolution behaviour of lipid monolayer- coated, air filled microbubbles: effect of lipid hydrophobic chain length*", Langmuir, 18, 9225-9233, 2002.

Chang, P.H., Shung, K.K. and Levene, H.B., "*Quantitative measurements of second harmonic Doppler using ultrasound contrast agents*", Ultrasound Med Biol, 22 (9), 1205-1214, 1996.

Chatterjee, D. and Sarkar, K., "*A Newtonian rheological model for the interface of microbubble contrast agents*", Ultrasound Med Biol, 29, 1749-1757, 2003.

Chatterjee, D., Shi, W.T., Sarkar, K. and Forsberg, F., "*Characterization of ultrasound contrast microbubbles using in vitro experiments and viscous and viscoelastic interface models for encapsulation*," J. Acoust. Soc. Am., 118 (1), 539-550, 2005.

Chen, W. S., Matula, T. J. and Crum, L. A., " *The disappearance of ultrasound contrast bubbles: observations of bubble dissolution and cavitation nucleation*", Ultrasound Med. Biol., 28(6), 793-803, 2002.

Chen, Q., Zagzebski, J., Wilson, T. and Stiles, T., "*Pressure-dependent attenuation in ultrasound contrast agents*," Ultrasound Med Biol, 28(8), 1041─1051, 2002.

Chen, W.S., Matula, T.J., Brayman, A.A. and Crum, L.A., "*A comparison of the fragmentation thresholds and inertial cavitation doses of different ultrasound contrast agents*", J. Acoust. Soc. Am., 113(1), 643-651, 2003.

Chomas, J.E., Dayton, P.A., May, D., et al, "*Optical observation of contrast agent destruction*", Appl. Phys. Lett., 77(7), 1056-1058, 2000.

Chomas, J.E., Dayton, P., Allen, J., Morgan, K. and Ferrara, K.W., "*Mechanisms of contrast agent destruction*", IEEE Trans. Ultrason., Ferroelect., Freq. Contr., 48(1), 232-247, 2001.

Church, C.C., "*The effects of an elastic solid surface layer on the radial pulsations of gas bubbles*", J. Acoust. Soc. Am., 97, 1510-1521, 1995.

Dayton, P.A., Morgan, K.E., Klibanov, A.L., Brandenburger, G.H., and Ferrara, K.W., "*Optical and acoustical observations of the effects of ultrasound on contrast agents*", IEEE Trans. Ultrason., Ferroelect., Freq. Contr., 46(1), 220-232, 1999.

de Jong, N., Hoff, L., Skotland, T. and Bom, N., "*Absorption and scatter of encapsulated gas filled microspheres: theoretical consideration and some measurements*", Ultrasonics, 30(2), 95- 103, 1992.

de Jong, N. and Hoff, L., "*Ultrasound scattering properties of Albunex microspheres*", Ultrasonics, **31**(3), 175-181, 1993.

de Jong, N., Cornet, R., and Lancèe, C.T., "*Higher harmonics of vibrating gas-filled microspheres. Part two: measurements*", Ultrasonics, 32(6), 455-459, 1994.

Edwards, D.A., Brenner, H. and D.T. Wasan," *Interfacial transport processes and rheology, Butterworth-Heinemann*", 1991.

Epstein, P. S. and Plesset, M.S., "*On stability of gas bubbles in Liquid-gas solutions*", J. Chem. Physics, 18, 1505-1509, 1950.

Evans, E. A. and Skalak, R. "*Mechanics and Thermodynamics of Biomembranes*", CRC Press, 1980.

Frinking, P.J.A. and de Jong, N., "*Acoustic modeling of shell-encapsulated gas bubbles*", Ultrasound Med. Biol., 24(4), 523-533, 1998.

Frinking, P.J.A., Boukaz, A., Kirkhorn, J., Ten Cate, F.J., and de Jong, N., "*Ultrasound contrast imaging: current and new potential methods*," Ultrasound Med. Biol., 26(6), 965-975, 2000.

Goldberg, B. B., Raichlen, J. S., and Forsberg, F., "*Ultrasound Contrast Agents: Basic Principles and Clinical Applications"*, 2nd Ed., Martin Dunitz, London, 2001.

Guan, J. and Matula, T.J., "*Using light scattering to measure the response of individual ultrasound contrast microbubbles subjected to pulsed ultrasound in vitro*", J. Acoust. Soc. Am., 113(1), 643-651, 2004.

Hoff, L., "*Acoustic characterization of contrast agents for medical ultrasound imaging*", Ph.D. thesis, Norwegian University of Science and Technology, 2000.

Hoff, L., Sontum, P.C., and Hovem, J.M., "*Oscillations of polymeric microbubbles: effect of the encapsulating shell*", J. Acoust. Soc. Am., 107(4), 2272-2280, 2000.

Kabalnov, A., Klein, D., Pelura, T., Schutt, E. and Weers, J. "*Dissolution of multicomponent microbubbles in the blood stream: 1. Theory*", Ultrasound Med. Biol., 24(5), 739-749, 1998.

Kabalnov, A., Bradley, J., Flaim, S., Klein, D et al., "*Dissolution of multicomponent microbubbles in the bloodstream: 2. Experiment*", Ultrasound Med. Biol., 24(5), 751-760, 1998.

Khismatullin, D.B. and Nadim, A., "*Radial oscillations of encapsulated microbubbles in viscoelastic liquids*", Phys. Fluids, 14(10), 3534-3557, 2002.

Klibanov, A.L., Ferrara, K.W., Hughes, M.S., et al, "*Direct video-microscopic observation of the dynamic effects of medical ultrasound on ultrasound contrast microspheres*", Invest. Radiol, 33(12), 863-870, 1998.

Klibanov, A.L., Hughes, M.S., Wojdyla, J.K., Wible, J.H., Jr., and Brandenburger, G.H., "*Destruction of contrast agent microbubbles in the ultrasonic field: The fate of the microbubble shell and the importance of the bubble gas content*", Acad. Radiol, 9(suppl 1), S41-S45, 2002.

Leighton, T.G., "*The Acoustic Bubble"*, Academic Press, San Diego, 1994.

Medwin, H., "*Counting bubbles acoustically: a review*," Ultrasonics, 15, 7-13, 1977.

Morgan, K.E., Allen, J. S., Dayton, P. A., Chomas, J. E., Klibanov, A. L., and Ferrara, K. W. ,"*Experimental and theoretical evaluation of microbubble behavior: effect of transmitted phase and bubble size*," IEEE Transaction on Ultrasonics, Ferroelectrics, and Frequency Control, 47(6), 1494-1509, 2000.

Moran, C.M., Anderson, T., Pye, S.D., Sboros, V. and Mcdicken, W.N., "*Quantification of microbubble destruction of three fluorocarbon-filled ultrasonic contrast agents*", Ultrasound Med. Biol., 26(4), 629-639, 2000.

Porter, T.R. and Xie, F., "Transient myocardial contrast after initial exposure to diagnostic ultrasound pressures with minute doses of intravenously injected microbubbles", Circulation, 92, 2391-2395, 1995.

Porter, T.R., Iversen, P.L., Li, S., et al, "*Interaction of diagnostic ultrasound with synthetic oligonucleotide-labeled perfluorocarbon-exposed sonicated dextrose albumin microbubbles*", J. Ultrasound Med., 15, 577-584, 1996.

Porter, T.R., Xie, F., Silver, M., Kricsfeld, D. and O'Leary, E., "Real-time perfusion imaging with low mechanical index pulse inversion Doppler imaging", J. Am. Coll. Cardiology, 37, 748-753, 2001.

Price, RJ, Skyba, DM, Kaul, S, et al, "*Delivery of colloidal particles and red cells to tissue through microvessel ruptures created by targeted microbubble destruction with ultrasound* ", Circulation, 98, 1264-1267, 1998.

Sarkar, K., and Prosperetti, A., "*Coherent and Incoherent scattering by oceanic bubbles*," Journal of Acoustical Society of America, 96, 332-341, 1994.

Sboros, V., Moran, C.M., Pye, D., Mcdicken, W.N., "*Contrast agent stability: A continuous B-mode imaging approach*", Ultrasound Med. Biol., 27(10), 1367-1377, 2001.

Sboros, V., Moran, C.M., Anderson, T. and Mcdicken, W.N., "*An in vitro study of a microbubble contrast agent using clinical ultrasound imaging system*", Phys Med Biol., 49, 159-173, 2004.

Shankar, P.M., Krishna, P.D., and Newhouse, V.L., "*Advantages of subharmonic over second harmonic backscatter for contrast-to-tissue echo enhancement*", Ultrasound Med Biol, 24(3), 395-399, 1998.

Shi, W.T., Forsberg, F., Hall, A.L. et al, "*Subharmonic imaging with microbubble contrast agents: initial results*", Ultrasound Imaging, 21, 79-94, 1999.

Shi, W.T. and Forsberg, F., "*Ultrasonic characterization of the nonlinear properties of contrast microbubbles*", Ultrasound Med Biol, 26(1), 93-104, 2000.

Shi, W.T., Forsberg, F., Tornes, A., Østensen, J. and Goldberg, B.B., "*Destruction of contrast microbubbles and the association with inertial cavitation*", Ultrasound Med. Biol., 26(6), 1009-1019, 2000.

Shohet, R.V., Chen, S., Zhou, Y.T., et al, "Echocardiographic destruction of albumin microbubbles directs gene delivery to the myocardium", Circulation, 101, 2554-2556, 2000.

Simpson, D.H., Chin, C.T. and Burns, P.N., "*Pulse inversion Doppler: a new method for detecting nonlinear echoes from microbubble contrast agents*", IEEE Trans. Ultrasonics, Ferroelectricity and Frequency Control, 46(2) 372-382, 1999.

Song, J, Ming, Q., Kaul, S. and Price, R.J., "Stimulation of arteriogenesis in skeletal muscles by microbubble destruction with ultrasound", Circulation, 106(12) 1550-1555, 2002.

Sonne, C, Xie, F., Lof, J., "*Differences in Definity and Optison microbubble destruction rates at a similar Mechanical Index with different real-time perfusion systems*", Am. Soc. Echocardiography, 16(11), 1178-1185, 2003.

Vanliew, H.D., Raychaudhari, S., J. appl. Physiol., 82, 2045-2053,1997.

Walker, K.W., Pantely, G.A. and Sahn, D.J., "Ultrasound-mediated destruction of contrast agents: Effect of ultrasound intensity, exposure and frequency", Investigative Radiology, 32(12), 728-734, 1997.

Wu, J. and Tong, J., "*Measurements of the nonlinearity parameter B/A of contrast agents*", Ultrasound Med Biol, 24(1), 153 ─ 159, 1997.

Zhang, D., Gong, X-F, Liu, J-H, et al, "*The experimental investigation of ultrasonic properties for a sonicated contrast agent and its application in biomedicine*", 26(2), 347-351, 2000.